2-2020

A Universal Model of Unsaturated Hydraulic Conductivity with Complementary Adsorptive and Diffusive Process Components

Arash Modaresi Rad
Boise State University

Bijan Ghahraman
Ferdowsi University of Mashhad

Abolfazl Mosaedi
Ferdowsi University of Mashhad

Mojtaba Sadegh
Boise State University

Water Resources Research

RESEARCH ARTICLE
10.1029/2019WR025884

A Universal Model of Unsaturated Hydraulic Conductivity With Complementary Adsorptive and Diffusive Process Components

Arash Modaresi Rad[1], Bijan Ghahraman[2], Abolfazl Mosaedi[2], and Mojtaba Sadegh[1]

[1]Department of Civil Engineering, Boise State University, Boise, ID, USA, [2]Water Engineering Department, College of Agriculture, Ferdowsi University of Mashhad, Mashhad, Iran

Key Points:
- A flexible hydraulic conductivity function is proposed that accounts for three fractal regimes
- This joint conductivity function embraces contributions of film and vapor flow with a new dispersion tortuosity factor
- Effectiveness of universal scaling for modeling water transport at low water content is compared with vapor conductivity model

Supporting Information:
- Supporting Information S1

Correspondence to:
M. Sadegh,
mojtabasadegh@boisestate.edu

Citation:
Modaresi Rad, A., Ghahraman, B., Mosaedi, A., & Sadegh, M. (2020). A universal model of unsaturated hydraulic conductivity with complementary adsorptive and diffusive process components. *Water Resources Research*, *56*, e2019WR025884. https://doi.org/10.1029/2019WR025884

Received 28 JUN 2019
Accepted 24 JAN 2020
Accepted article online 26 JAN 2020

Abstract Accurate estimation of unsaturated hydraulic conductivity (HC) is one of the most challenging problems in soil science. Here, we propose a novel approach to model HC using percolation theory. Transient behavior of water transport phenomena at low moisture contents requires additional physical process representation, beside capillary conductivity, to ensure accurate prediction of unsaturated HC. We augment the capillary model from percolation theory with two additional components, namely, (1) film flow, which is the product of volumetric flow rate per perimeter by specific perimeter of solid particles, and (2) isothermal vapor HC, derived from the Fick's law of vapor diffusion and relative humidity. The fractal characteristics of last fractal regime are used to model tortuosity and ultimately HC of vapor flow. Since the typical pressure head range of universal scaling from percolation theory is analogous to the range of vapor flow, we demonstrate that the universal scaling presented in previous studies is not sufficient to model HC for water contents below a crossover point. We also, by analyzing the scaled water retention properties, demonstrate that most studied soils exhibit three fractal regimes. Therefore, a piecewise HC function of capillary flow is developed to account for three fractal regimes, providing more flexibility for soils with multimodal characteristics. The proposed joint HC function is more accurate compared to the model of Peters-Durner-Iden and predecessor percolation theory models.

1. Introduction

Arguably, the most widely used methodology to model transient water and solute transport is Richards' equation, which requires prior information regarding water retention characteristic and hydraulic conductivity (HC) properties (Sadeghi et al., 2012). Accurate estimation of unsaturated HC is in turn one of the most challenging topics in vadose zone hydrology (Or & Assouline, 2013). HC plays an important role in the transport of pollutants and nutrients and hence impacts water quality. Examples of such impacts include movement of pesticides and nutrients through soil and thereby contamination of water resources (Birdsell, Rajaram, & Lackey, 2015; Birdsell, Rajaram, Dempsey, & Viswanathan, 2015b; Durner, 1994; Tiktak et al., 2012; Vink et al., 1997), as well as oil recovery by spontaneous imbibition of water as a mechanism for oil recovery (Allred & Brown, 1994; Birdsell, Rajaram, Dempsey, & Viswanathan, 2015a), among many more.

Since measurement of unsaturated HC is heavily time demanding, especially at low water contents where transitivity of flow occurs at slow rates, one of the most convenient and cost-effective ways to predict unsaturated HC is to use water retention characteristics along with direct measurement of saturated HC (Weber et al., 2017). This methodology was first portrayed in a work by Purcell (1949), and further developments were continued afterward by numerous authors, including Childs and Collis-George (1950), who introduced bundle of intersecting cylindrical capillary tubes (cut and random rejoin model); Fatt and Dykstra (1951) and Burdine (1953), who added a tortuosity factor in the Purcell (1949) model; and Wyllie and Gardner (1958), Mualem (1976a), and others. Once soil pore space geometry was defined in each model, Hagen-Poiseuille law was used to deduce relative HC from a water retention model. In order to find an integrable expression of fluid movement, earlier studies simplified the complex geometry of soil pore space and described pore space as a bundle of cylindrical parallel tubes. Thus, in the capillary bundle of tubes model, size of each tube (pore) is considered proportional to a certain particle size (Arya & Paris, 1981). Although the geometry of pore space was simplified in the capillary bundle models (Burdine, 1953; Mualem, 1976b), the derived models managed to give a fairly accurate description of HC at high water contents where

capillary forces are dominant. However, these early models underestimate permeability at low water contents (Sakai et al., 2009). This comes as no surprise since assumptions of the parallel bundle of capillary tubes are rarely adequate considering crookedness of paths in the soils' complex geometry and interconnections between pores of different radii. Hunt, Ghanbarian, et al. (2013), Hunt, Ewing, et al. (2013) discussed some major shortcomings of the capillary bundle models, including lack of consideration of flow movement in any given direction, neglecting cross-connections between the tubes, and lack of accessibility constraints for pores. The authors also criticized adjustments later made into the capillary bundle model (which introduced a tortuosity factor to compensate for the complex geometry of soil) and argued that such fundamental errors should not be accepted and used, to begin with.

Fractals can be described as iterative geometrical models for describing irregular and fragmented systems, and given that the degree of irregularity in a porous medium is independent of scale, transport of fluid can be modeled by theories arising from fractal concepts. Fractal models assume soil as a hierarchical system, making them a suitable tool to represent tortuosity of heterogeneous soil structure. Studies by Jacquin and Adler (1985), Ross (1986), Tyler and Wheatcraft (1990), and Rieu and Sposito (1991) were the earliest fractal models of water retention function (WRF) and soil permeability. Fuentes et al. (1996) derived a fractal-based HCF from their retention model; however, their model was not verified by actual measurements of HC. As Gimenez et al. (1997) discussed, the theoretical range of fractal dimension from Fuentes et al. (1996) model is quite narrow compared with those obtained from measurements, and hence, a vague morphological interpretation of fractal dimension is inferred from their model. Shepard (1993) utilized fractal geometry of the Koch curve (to represent tortuosity) combined with Poiseuille's equation to propose a hydraulic conductivity function (HCF). Following previous work by Li and Horne (2005), Li (2010) derived the Purcell and Brooks and Corey permeability models for both drainage and imbibition processes on the basis of their newly developed WRF. Although the new relative HCF by Li (2010) significantly improved fit over the three studied rock samples compared to the conventional model of Brooks and Corey, predictions were still biased toward the wet end for both water and steam experiments. Alfaro Soto et al. (2017) utilized the fractal model of water retention previously introduced by Soto and Vilar (2006) combined with the approaches of Mualem (1976a) and Burdine (1953) to derive formulations for unsaturated HC; however, their model is not very flexible and does not take into account multifractal characteristics observed in some soils.

Percolation theory has also been proven successful to model two-phase flow and estimation of HC in porous media (Blunt et al., 1992; Helba et al., 1992; Larson et al., 1981). Critical path analysis was developed on the basis of percolation theory with an assumption that pore throats control flow in a heterogeneous porous medium. Hunt (2001) was first to successfully utilize critical path analysis to develop an HCF, and model flow movement in complex networks. Ever since, numerous studies including Hunt and Gee (2002a, 2002b), Hunt (2004a, 2004b), Ghanbarian-Alavijeh and Hunt (2012), Hunt, Ghanbarian, et al. (2013), Hunt, Ewing, et al. (2013), Ghanbarian, Hunt, and Daigle (2015), and ModaresiRad et al. (2019) further improved his work. However, the proposed models only account for capillary forces, and as a result, it is expected that they diverge significantly from observed measurements at high pressure heads. From mid-ranges to fully saturated, soil capillary flow dominates HC, and pore necks essentially control the degree of transitivity of fluid in porous media, making the role of pore body surface area and relative surface forces inconsiderable, whereas in much lower degrees of saturation, circumstances are reversed (Figure 1). Other studies by Tuller, Or, and Dudley (1999), Zand-Parsa and Sepaskhah (2004), and Zand-Parsa (2006) have shown that specific liquid-vapor interfacial area around soil particles can be used to improve prediction of unsaturated HC as well. Figure 1 illustrates a schematic representation of the liquid-vapor interfacial area as a function of applied pressure head for different soil textures. As depicted in Figure 1, different mechanisms of water transport can be observed at different stages of applied pressure head.

As pointed out by several authors including Tuller and Or (2001), Goss and Madliger (2007), Lebeau and Konrad (2010), and Jansik et al. (2011), the earlier models of HC lack the required flexibility to portray the correct functional shape of HC at high pressure heads (e.g., Brooks & Corey, 1966; Ippisch et al., 2006; Kosugi, 1996; Van Genuchten, 1980). Water flow movement through soil in forms of water menisci, water films, and water vapor can be fully described once coexistence of capillary, adsorptive, and diffusive components of flow are factored into the modeling effort. Philip (1977) considered the liquid-vapor interface of two-phase flow at relatively low water contents as a surface of constant partial specific Gibbs free energy

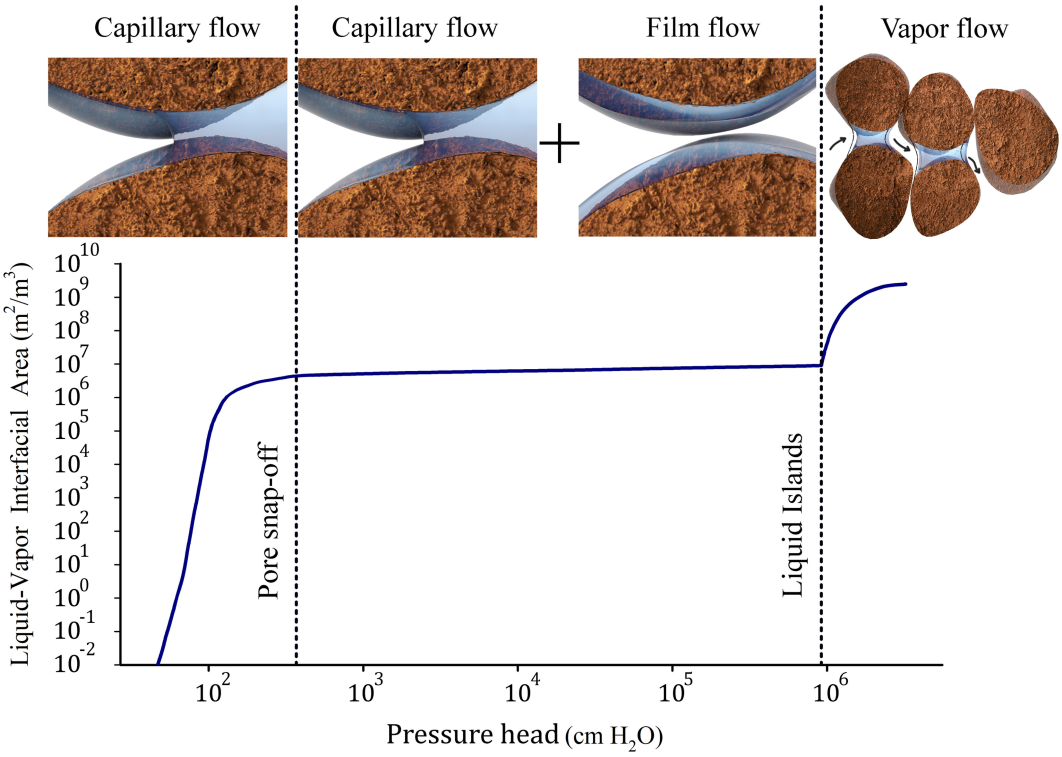

Figure 1. Schematic representation of the liquid-vapor interfacial area as a function of applied pressure head and underlying processes involved in water transmissivity, adopted from by Tuller et al. (1999).

(chemical potential) and introduced an adsorptive (A) and a capillary (C) term to describe the chemical potential. Thus, chemical potential (Π) was described as

$$\Pi = \mathrm{A(d)} + \mathrm{C(k)} = -\lambda\frac{RT}{d} - \frac{2\sigma k}{\rho}, \tag{1}$$

where $-\lambda RT/d$ signifies an empirical adsorption term introduced by Philip (1977) and $-2\sigma k/\rho$ represents classical Young-Laplace equation. These two elements are collectively known as augmented Young-Laplace equation. λ is a constant equal to 10^{-10}(m), R is gas constant ($JK^{-1}kg^{-1}$), T is temperature (K), d is normal distance of interface from solid, σ is surface tension at the interface (Nm^{-1}), ρ is density of liquid (kgm^{-3}), and k is liquid-vapor interface mean curvature (°). However, in this model, the film thickness was determined from the joint contributions of adsorptive and capillary terms (equation (1)). The adsorptive component can be defined as a thermodynamic process of adsorption of liquid vapor molecules onto either solid or liquid layer. Tuller and Or (2001) used the interface concepts developed by Derjaguin (1987a, 1987b) and Iwamatsu and Horii (1996) to develop a model that incorporates adsorptive and capillary terms. Unlike the approach used in Philip (1977), they calculate film thickness solely based on the adsorptive term and introduced shifted Young-Laplace equation. Ever since, several adjustments have been made to further develop the physical model of Or and Tuller (2000), including solving the flexibility issue and simplifying the original WRF and HCF by Lebeau and Konrad (2010), taking pore-scale hysteresis and contact angle effect into account by Diamantopoulos and Durner (2013), and adjusting the film HC model to incorporate effects of surface roughness by Zheng et al. (2015). Fredlund and Xing (1994) proposed a model, without dividing contribution of capillary and film flow, that improved the estimation of unsaturated HC at the dry end. However, their model does not lead to a closed-form equation, and a numerical solution is required to determine the relative HCF (Kebre et al., 2017). By applying even more pressure and at very low saturation, water pathways become longer and sparse, which in turn limit the connectivity of liquid, and as a result, water movement is only viable through vapor flow (Kelleners et al., 2016; Lehmann et al., 2008; Shokri & Or, 2010). Assuming that gradient in gravitational potential is insignificant in vapor flow, Philip

and De Vries (1957), Mehta et al. (1994), and Saito et al. (2006) described isothermal vapor HC. Subsequent studies have shown that isothermal vapor conductivity can be added to liquid conductivity to represent the total range of unsaturated HC (Peters, 2013; Rudiyanto et al., 2015; Sakai et al., 2009).

A comprehensive literature review indicates that fractal formulation of soil-water conductivity of all the previous approaches was either applicable to a certain group of soil textures or the proposed models lacked the flexibility to portray an entire range of water content. Pioneering studies by Hunt (2001) and Hunt (2004a, 2004b) on the application of percolation theory for water retention and HC of soils led to new pathways for modeling fluid transport in soils. Later studies by Ghanbarian-Alavijeh and Hunt (2012), Hunt, Ghanbarian, et al. (2013), Hunt, Ewing, et al. (2013), and Ghanbarian et al. (2016) further improved model predictions by introducing irregular rough pore cross sections and bimodal pore size distribution. Despite the adjustments made, these models slightly underestimate at high saturations and underestimate or overestimate at low saturation (ModaresiRad et al., 2019). Other studies including Tuller and Or (2001), Lebeau and Konrad (2010), and Rudiyanto et al. (2015) have shown that in order to adequately describe processes of water transport in an entire range of water content, the adsorptive and diffusive components of liquid conductivity should be considered as well. This paper builds upon the progress made in the literature and advances the existing models. Contributions of this paper include the following:

1. We propose an extended HCF by enhancing model flexibility for soils with multimodal characteristics. We assume that there are multiple (up to two) changepoints in the pore-size distribution of soil and the pore space can be divided into several distinct regions where the parameters of pore solid fractal (PSF) model (Bird, Perrier, & Rieu, 2000) that define physical characteristics of soil and determine the rate of solute movement in soil are significantly different from one another. Previously, Hunt, Ghanbarian, et al. (2013), Hunt, Ewing, et al. (2013) developed a multifractal HC for soils with two fractal regimes; we further extend their method by including a third fractal regime. This is achieved by formulating the porosities of each regime, based on which the WRF is derived. Then, the proposed water retention model is used in the framework of critical path analysis from the percolation theory to derive the unsaturated HCF. Unlike the HCF of Hunt, Ghanbarian, et al. (2013), Hunt, Ewing, et al. (2013), we define the locations of changepoints prior to solving the inverse problem. The scaled form of the PSF model (Bird et al., 2000) was used for analyzing changes in the slope of water retention data, and the adjusted maximal two-sample *t* test introduced in ModaresiRad et al. (2019) was used to identify the most probable location of changepoint.
2. We further adjust the HC model by proposing a joint HCF that minimizes the limitations imposed by capillary movement at low water contents. The role of an adsorptive component of liquid flow in porous medium comes into play as a snap-off mechanism takes place and liquid is spontaneously redistributed. At this stage, liquid movement through soil happens in the form of thin absorbed films, and therefore, the contribution of film flow is added to the total HC. Finally, the soil becomes dry enough so that the liquid continuity breaks and liquid islands begin to form. Hence, vapor diffusion controls the rate of liquid movement and is used as the last component of the unsaturated HCF, which is combined with adsorptive and capillary components to generate the total HCF. Predictive accuracy of the proposed joint model is then compared to the HC models of predecessor percolation theory by Ghanbarian et al. (2016) and the Peters-Durner-Iden (PDI) model (Iden & Durner, 2014).
3. We propose a new tortuosity factor for gas transport based on the model developed by Moldrup et al. (1999), reformulated in terms of fractal dimension of the last fractal regime. This tortuosity factor is used to describe diffusivity and isothermal vapor HC based on the methodology described in Saito et al. (2006). Universal scaling from percolation theory state that conductivity can be written as a universal power law scaling near the percolation threshold in moisture ranges where typically vapor flow dominates the conductivity. Application of universal scaling for modeling unsaturated HC is present in works of Ghanbarian-Alavijeh and Hunt (2012), Ghanbarian, Hunt, and Daigle (2015), Ghanbarian, Hunt, Skinner, et al. (2015), and Ghanbarian et al. (2016); however, the actual pressure head range of the data sets used in these studies was not appropriate to validate the universal scaling model (contributions of universal scaling and vapor flow are generally dominant at high pressures, roughly 2,000 kPa and beyond). Hence, the effectiveness of universal scaling approach for saturations below the crossover point in which universal percolation scaling takes over the critical path analysis is compared to the performance of the vapor HC model, and further discussions are made.

2. Methods

2.1. Water Retention and HC Data

In this study, 11 published data sets from the literature with a wide variety of textures are used to assess the performance and goodness-of-fit of the proposed model. Selected data include measurements of water retention and HC, encompassing measurements at high pressures. The data set is composed of Shonai Sand referenced by Soil Code 1 (Mehta et al., 1994); Sandy Loam, and Clay Loam referenced by Soil Codes 2 and 3, respectively (Tuller & Or, 2001); Silt Loam referenced by Soil Code 4 (Zhang, 2010); Gilat Loam, Masa Loamy Sand, Adelanto Loam, Hollern Clay 1, Pachapa Loam, and Pachapa fine Sandy Clay referenced by Soil Codes 5, 7, 8, 9, 10, and 11, respectively (Wang et al., 2016); and Plumhof I sand referenced by Soil Code 6 (Leij, 1996). This data set is particularly suited for investigating the effectiveness of a joint capillary, adsorptive, and diffusive HC model.

2.2. Capillary Conductivity Model

Liquid retention and HC vary as a function of the proportion of gas and liquid that are accumulated in the soil pores (Buckingham, 1907). On the basis of previous pioneering studies on percolation theory (Hunt, 2001; Hunt & Gee, 2002a), Hunt (2004a, 2004b) provided a theoretical framework for prediction of HC that can be computed based on the PSF model of water retention curve developed by Perrier et al. (1999) and modified by Bird et al. (2000). Percolation theory can be defined as a framework that quantifies connections of randomly arranged volume, area, or line segments (Hunt, 2001). Hunt and Gee (2002b) used particle size distribution data to estimate HC and accounted for the bimodality of some soil samples. To include the effects of pore solid interface roughness of cross-sectional area and roughness of pore along a tube, Ghanbarian et al. (2016) modified the power term of relation between hydraulic conductance and pore radius. Although the considered surface roughness term enhanced model performance, as demonstrated in ModaresiRad et al. (2019), the model slightly underestimates HC near saturation and greatly underestimates HC from middle to dry ranges of saturation. Hence, the proposed methodology in ModaresiRad et al. (2019) is used herein to predict HC. We further extend HCF to account for up to three fractal regimes. The scaled form of the PSF model (Bird et al., 2000) is used for analyzing changes in the slope of water retention data and is formulated as

$$\log\theta^* = \log\frac{\theta+\beta-\phi}{\beta}, \tag{2}$$

where θ^* is scaled volumetric water content, θ is volumetric water content, $\beta = p/(p+s)$ is PSF parameter (p and s represent proportions of soil total region occupied by pores and solids, respectively), and ϕ is total porosity. Then, a log-log curve of θ^* versus (h_{min}/h) is used for changepoint analysis, where h is pressure head and h_{min} is pressure head corresponding to desaturation of largest pore. Slope of the log-log curve of θ^* versus (h_{min}/h) is equivalent to fractal dimension subtracted by three. This is equivalent to the negative Hurst exponent, indicating the state of pore size distribution (roughness). Following the changepoint detection procedure described in ModaresiRad et al. (2019), two series of $\{\theta_t^*\}(t=1,...,N)$ and $\{(h_{min}/h)_t\}(t=1,...,N)$ are defined, and the T_{max} test statistic is used to locate changepoints. The null hypothesis for this test is defined as

$$H_0 : \left\{\theta_t^*, \left({}^{h_{min}}/_{h}\right)_t\right\} \sim F(\mu,\sigma^2), \tag{3}$$

in which, F represents normal distribution with mean μ and variance σ^2. In words, null hypothesis states that there are no changepoints in the slope generated by the two series. Alternative hypothesis states that there is a changepoint and considers that the slopes of the two intervals are significantly different from one another:

$$H_a : \begin{cases} \{\theta_t^*, (h_{min}/h)_t\} \sim F(\mu_1,\sigma^2), t=1,...,k, \\ \{\theta_t^*, (h_{min}/h)_t\} \sim F(\mu_2,\sigma^2), t=k+1,...,N. \end{cases} \tag{4}$$

Accordingly, the test statistic for detection of changepoint can be written as

$$T_{max} = \max_{1\le k\le N-1} \frac{1}{\widehat{\sigma}_k}\left[\frac{k(N-k)}{N}\right]^{\frac{1}{2}}\left|\left(\left(\frac{1}{k}\sum_{1\le t\le k}\theta_t^* - \frac{1}{N-k}\sum_{k+1\le t\le N}\theta_t^*\right)^2 + \left(\frac{1}{k}\sum_{1\le t\le k}(h_{min}/h)_t - \frac{1}{N-k}\sum_{k+1\le t\le N}(h_{min}/h)_t\right)^2\right)^{\frac{1}{2}}\right|, \quad (5)$$

where, k is the most probable value of numerator for which the difference between the slope of water retention for values smaller than k and for values greater than k is significantly different from the rest, N is the length of data, and $\widehat{\sigma}_k$ is defined as

$$\widetilde{\sigma}^2 = \frac{1}{N}\left[det\begin{pmatrix} Var(\theta_t^*) & Cov(\theta_t^*, (h_{min}/h)_t) \\ Cov((h_{min}/h)_t, \theta_t^*) & Var((h_{min}/h)_t) \end{pmatrix}\right]. \quad (6)$$

According to Hunt, Ghanbarian, et al. (2013), Hunt, Ewing, et al. (2013), one would expect the percolation threshold (θ_t) to be finite once textural pores are present in medium; value of which originally was set to zero. However, in our study, we set this value equal to the lowest available measurement of saturation. Alternatively, according to the results obtained for a wide variety of soil textures from Tuller and Or (2005) and Or and Tuller (1999), a matric potential (build up potential as a result of both capillary and adsorptive forces, ignoring solid-liquid interface drag forces as well as gravitational forces) value of −10 MPa typically defines the limit of contribution of capillary flow. Accordingly, θ_t would be less than joint porosities of first and second regimes. Here, we expand the HCF to account for two changepoints (Points $k1$ and $k2$). Figure 2 illustrates the water retention curve of Shonai Sand that has three regions with distinct fractal characteristics. The parameters of first, second, and third regimes are tuned by considering the entire range of water retention data, water retention data from Point $k1$ to last available measurement, and water retention data from Point $k2$ to last available measurement, respectively. Tuning parameters of each regime against data from beginning of the regime to the last available measurement is justified due to use of parameters ϕ (porosity) and β (ratio of all pores and solids that contribute to flow of liquid). Trimming pores and solids below a certain pressure head results in spurious computation of these two parameters.

The proposed piecewise multifractal PSF soil WRF is derived as (see Appendix A for derivation)

$$\theta = \begin{cases} \phi, & h<h_{min} \\ \phi-\beta_1\left[1-\left[\frac{h}{h_{min}}\right]^{D_1-3}\right], & h_{min}<h<h_{k1} \\ \phi_2+\phi_3-\beta_2\left[1-\left[\frac{h}{h_{k1}}\right]^{D_2-3}\right], & h_{k1}<h<h_{k2} \\ \phi_3-\beta_3\left[1-\left[\frac{h}{h_{k2}}\right]^{D_3-3}\right], & h_{k2}<h<h_{max} \end{cases} \quad (7)$$

The piecewise multifractal relative unsaturated HCF based on equation (7) is described as (see Appendix A for derivation)

$$K_r^{cap} = \frac{K\theta}{K_s\theta} = \begin{cases} \left[\frac{\beta_1-\phi+\theta-\theta_t}{\beta_1-\theta_t}\right]^{\frac{\lambda_1}{3-D_1}}, & \theta-\theta_t>\phi_2+\phi_3 \\ \frac{\beta_1^{\frac{\lambda_1}{3-D_1}}}{\beta_2^{\frac{\lambda_2}{3-D_2}}}\left\{\frac{\beta_1-\phi_1}{\beta_1}^{\frac{\lambda_1}{3-D_1}}\left[\frac{\beta_2-\phi_2+\theta-\theta_t}{[\beta_1-\theta_t]^{\frac{\lambda_1}{3-D_1}}}\right]^{\frac{\lambda_2}{3-D_2}}\right., & \phi_3<\theta-\theta_t<\phi_2+\phi_3 \\ \frac{\beta_1^{\frac{\lambda_1}{3-D_1}}}{\beta_3^{\frac{\lambda_3}{3-D_3}}}\left\{\frac{\beta_1-\phi_1}{\beta_1}^{\frac{\lambda_1}{3-D_1}}\left\{\frac{\beta_2-\phi_2}{\beta_2}^{\frac{\lambda_2}{3-D_2}}\left[\frac{\beta_3-\phi_3+\theta-\theta_t}{[\beta_1-\theta_t]^{\frac{\lambda_1}{3-D_1}}}\right]^{\frac{\lambda_3}{3-D_3}}\right.\right. & \theta-\theta_t<\phi_3 \end{cases} \quad (8)$$

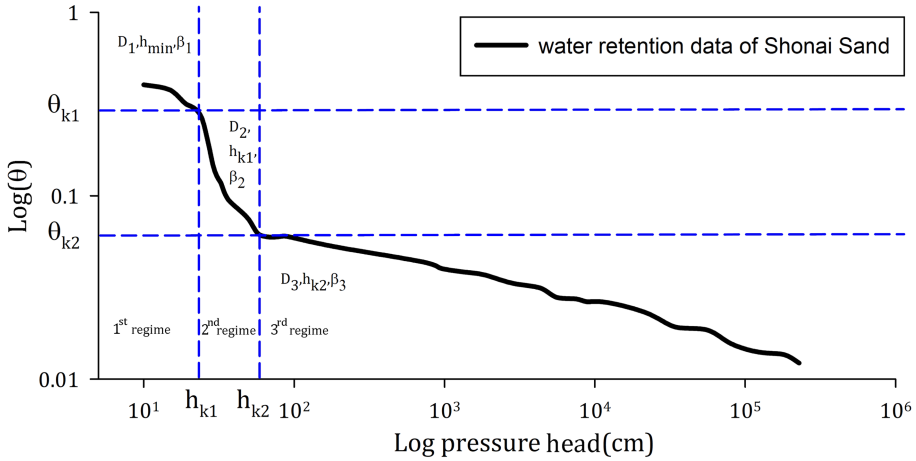

Figure 2. Water retention curve of Shonai Sand (Soil Code 1) with three fractal regimes.

Similarly, for cases that measurement of saturated HC is not available, we have

$$K_r^{cap}=\frac{K\theta}{K\theta'}=\begin{cases}\left[\dfrac{\beta_1-\phi+\theta-\theta_t}{\beta_1-\phi+\theta'-\theta_t}\right]^{\frac{\lambda_1}{3-D_1}}, & \theta-\theta_t>\phi_2+\phi_3\\ \dfrac{\beta_1^{\frac{\lambda_1}{3-D_1}}}{\beta_2^{\frac{\lambda_2}{3-D_2}}}\left\{\dfrac{\beta_1-\phi_1}{\beta_1}\right\}^{\frac{\lambda_1}{3-D_1}}\dfrac{[\beta_2-\phi_2+\theta-\theta_t]^{\frac{\lambda_2}{3-D_2}}}{[\beta_1-\phi+\theta'-\theta_t]^{\frac{\lambda_1}{3-D_1}}}, & \phi_3<\theta-\theta_t<\phi_2+\phi_3\\ \dfrac{\beta_1^{\frac{\lambda_1}{3-D_1}}}{\beta_3^{\frac{\lambda_3}{3-D_3}}}\left\{\dfrac{\beta_1-\phi_1}{\beta_1}\right\}^{\frac{\lambda_1}{3-D_1}}\left\{\dfrac{\beta_2-\phi_2}{\beta_2}\right\}^{\frac{\lambda_2}{3-D_2}}\dfrac{[\beta_3-\phi_3+\theta-\theta_t]^{\frac{\lambda_3}{3-D_3}}}{[\beta_1-\phi+\theta'-\theta_t]^{\frac{\lambda_1}{3-D_1}}}. & \theta-\theta_t<\phi_3\end{cases} \tag{9}$$

The unimodal relative unsaturated HCF of Ghanbarian et al. (2016) is expressed as

$$K_r=\frac{K\theta}{K_s\theta}=\begin{cases}\left[\dfrac{\beta-\phi+\theta-\theta_t}{\beta-\theta_t}\right]^{\frac{\lambda}{3-D}}, & \theta_x<\theta<\theta_s\\ \left[\dfrac{\beta-\phi+\theta_x-\theta_t}{\beta-\theta_t}\right]^{\frac{\lambda}{3-D}}\left[\dfrac{\theta-\theta_t}{\theta_x-\theta_t}\right]^2, & \theta_t<\theta<\theta_x\end{cases} \tag{10}$$

with the corresponding water retention model of

$$\theta=\phi-\frac{p}{p+s}\left\{1-\left(\frac{h}{h_{min}}\right)^{D-d}\right\}, \tag{11}$$

where the roughness dimension was assumed to be $\lambda=2(4-D)-(3-D)/(2D-3)$ and θ_x is a crossover point where universal percolation scaling becomes dominant. According to Hunt (2004a, 2004b) and Hunt and Skinner (2005), θ_x can be approximated as

$$\theta_x=\theta_t+\left[\frac{2(\beta-\phi)}{\frac{\lambda}{3-D}-2}\right]. \tag{12}$$

The predecessor model (equation (10); Ghanbarian et al., 2016) will be compared with the proposed bimodal and multimodal unsaturated HC model (equations (A21) and (8), respectively) to determine effectiveness of

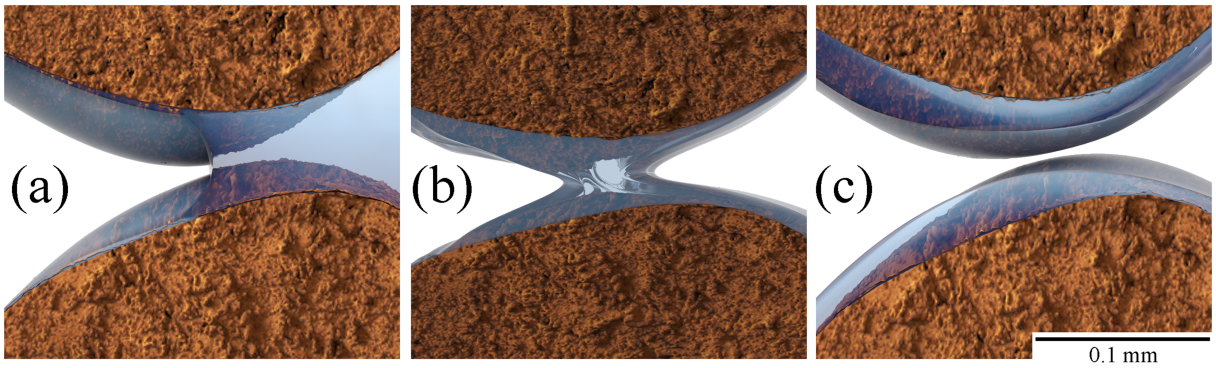

Figure 3. Displacement of water during pore drainage. (a) Pistonlike displacement during capillary flow. (b) The onset of pore snap-off. (c) Water movement through a flat liquid film with a certain thickness corresponding to its relevant pressure head.

the proposed capillary conductivity model as well as the universal percolation scaling in modeling water movement at low water contents. Note that the PSF soil water retention model used in this study only describes the capillary component and is used to model the capillary HC. This does not represent film or vapor conductivities.

2.3. Adsorptive Conductivity Model

As water is drained from pores, snap-off mechanism (spontaneous redistribution of liquid) takes place (illustrated in Figure 3).

Tokunaga (2009) found that in close packing of monodispersed spherical grains with zero contact angle, critical potentials at which water meniscus forms and disappears are equal to $\Psi_c \approx -9.1\sigma/d$ and $\Psi_d \approx -26\sigma/d$, respectively, where σ is surface tension and d is pore diameter. Thereby, for both cases of imbibition and drainage, conduction through absorbed films is dominant below Ψ_c and Ψ_d potentials, respectively. There have been numerous studies devoted to approximation of exact value of film conductivity and its contribution to total HC including, but not limited to, Mason and Morrow (1986), Derjaguin (1987a, 1987b), Derjaguin (1992), Derjaguin and Churaev (1992), Tuller et al. (1999), Tokunaga (2009), Lebeau and Konrad (2010), Zhang (2011), Peters (2013), and Wang et al. (2013). These studies infer that film conductivity depends on numerous factors, such as soil surface roughness (Zheng et al., 2015), surface charge (Lebeau & Konrad, 2010), ionic strength of fluid (Langmuir, 1938), and pore size distribution (Tokunaga, 2009). By considering an isothermal process, the difference between pressure in gas phase P_g and pressure in bulk liquid phase P_o can be described by disjoining pressure that is a function of film thickness (Derjaguin, 1987a, 1987b),

$$\Pi(\delta) = P_g - P_o, \tag{13}$$

where Π is derivative of Gibbs energy per unit area known as disjoining pressure, which to some extent is independent of curvature of the interface between film and air, and its relation to pressure head (h_m) can be described by $\Pi(\delta) = -h_m\rho g$, where ρ is density of fluid, g is gravitational acceleration, and δ is film thickness. Intermolecular and surface forces in an isothermal condition define overall disjoining pressure, and it is assumed that surface forces consist of four major components including ionic-electrostatic, molecular (van der Waals), structural, and adsorptive elements (Derjaguin, 1987a, 1987b; Lebeau & Konrad, 2010). However, the effects of ionic-electrostatic and molecular forces are often used to describe disjoining pressure, which can be defined as

$$\Pi(\delta) = \Pi_e(\delta) - \Pi_m(\delta), \tag{14}$$

in which Π_e and Π_m are ionic-electrostatic and molecular components of disjoining pressure, respectively. On the other hand, the relation between ionic-electrostatic disjoining pressure and film thickness was described by Langmuir (1938) through solving the Poisson-Boltzmann equation for a low-concentration symmetric ionic solution with a high potential substrate,

$$\Pi_e(\delta) = \frac{\varepsilon_r \varepsilon_o}{2}\left(\frac{\pi k_B T}{eZ}\right)^2 \frac{1}{\delta^2}, \tag{15}$$

where ε_r is relative permittivity of water (78.54), ε_o is permittivity of free space (8.85×10^{-12} $C^2J^{-1}m^{-1}$), k_B is Boltzmann constant (1.381×10^{-23} JK^{-1}), T is absolute temperature (298.15 K), e is electron charge (1.602×10^{-19} C), and Z is valence change (set to one). In addition, Iwamatsu and Horii (1996) described the relation between the molecular component (van der Waals forces) of disjoining pressure and film thickness as

$$\Pi_m(\delta) = \frac{A_{svl}}{6\pi\delta^3}, \tag{16}$$

where A_{svl} (J) is Hamaker constant for solid-vapor interactions through the intervening liquid. Tuller and Or (2005) noted that although the value of Hamaker constant ranges from -10^{-19} to -10^{-20}J, in real soil medium, this value is biased due to the formation of a diffuse double layer and the existence of heterogeneity in surface geometry. They proposed an adjusted value of -6×10^{-20}J to account for van der Waals and ionic electrostatic forces as well as the formation of diffuse double layer and surface roughness. On the other hand, recent studies by Resurreccion et al. (2011) and Wang et al. (2017) on a variety of soil textures have shown that the value of -10^{-20}J is more appropriate for calculation of thickness of monolayer water film. In physically based models of HC, the obtained film thickness is then used to derive unsaturated HC. Nonetheless, there have been numerous attempts to model film flow without preserving the physical characteristics of the film conductivity. This simplification was justified by minimizing the computational effort through introducing arbitrary parameters with no/semiphysical interpretations. These models often incorporate a logarithmic and/or power function to account for adsorptive water content in their WRF (Campbell & Shiozawa, 1994; Fayer & Simmons, 1995; Groenevelt & Grant, 2004; Iden & Durner, 2014; Khlosi et al., 2008; Peters, 2013; Rossi & Nimmo, 1994; Schneider & Goss, 2012) and derive HCF on the basis of water retention model.

In this study, the film HC model of Lebeau and Konrad (2010) is used to describe the adsorptive component. They described the HC of film by defining the Darcy-Buckingham flux per bulk cross section of porous media obtained from multiplying volumetric flow rate per perimeter by the specific perimeter of monodisperse sample of spherical particles,

$$K_r^{ads} = \frac{K^{ads}}{K_s} = \begin{cases} \frac{1}{K_s}\left[\frac{4\rho g}{\pi\eta D}[1-\phi]\delta^3\right], \delta \geq 10\text{nm} \\ \frac{1}{K_s}\left[\frac{\rho g B}{\pi\eta D}[1-\phi]\right], \delta < 10\text{nm} \end{cases} \tag{17}$$

where B accounts for film thickness as a function of temperature,

$$B = \left(4\delta^3 - 5a\delta^2 - a^2\delta\right)\exp\left(-\frac{a}{\delta}\right) - \left(6a^2\delta + a^3\right)Ei\left(-\frac{a}{\delta}\right), \tag{18}$$

in which $a = (1.621 \cdot 10^{-7})/T$ (m) and $Ei(-x) = -\int_x^{\infty}\left[\frac{\exp(-t)}{t}\right]dt$ can either be evaluated using Taylor series or can be solved through numerical methods. To generalize their model, Lebeau and Konrad (2010) replaced D with equivalent diameter D_e, which is the diameter of a spherical particle whose surface area per unit volume of monodisperse sample is equal to that of a polydisperse sample,

$$D_e = \frac{6}{\frac{\theta_m}{(1-\phi)}\left(\frac{A_{svl}}{6\pi\rho g h_{m,m}}\right)^{-1/3}}, \tag{19}$$

where θ_m is volumetric water content at pressure head $h_{m,m}$ in which capillary condensation due to surface roughness can be ignored, hence Lebeau and Konrad (2010) set $h_{m,m}$ to -10^3 m.

2.4. Diffusive Conductivity Model

Once snap-off mechanism occurs in pores and slits, liquid flows in form of thin adsorbed films, and this allows nonwetting liquid to pass freely through pore network. As the adsorbed layer of liquid becomes

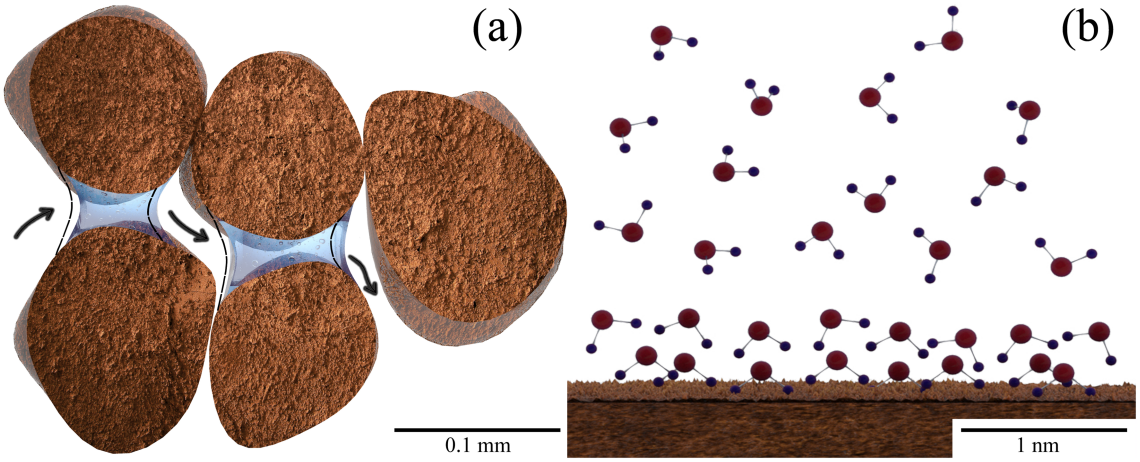

Figure 4. Representation of water movement mechanism at low moisture contents: (a) schematic representation of vapor movement mechanism among liquid islands; (b) formation of a double layer of water molecules in the vicinity of negatively charged soil solid particles, where small spheres (blue colored) represent positively charged hydrogen molecules and large spheres (red colored) are negatively charged oxygen molecules.

thinner, vapor transport starts governing the liquid movement. Vapor flow through soil was first explored by Penman (1940) who used Fick's law to develop his model. Later, mathematical relations of liquid water, water vapor, and heat movement in soil were reported by Philip and De Vries (1957), who explained and modeled the vapor movement and its interactions with liquid island. Disposition of liquid at dry soil was described by introducing a mechanism for vapor movement at relatively low moisture contents through the notion of liquid islands, where wetting liquid accumulates between grains (like an island) in an isolated state and thereby forms wedges in spaces between the solid particles. Consequently, as shown in Figure 4a assuming vapor flux direction is from left to right side, condensation and evaporation occur at the left and the right sides of the liquid islands, respectively. At higher pressures, as discussed in Israelachvili (2011), there remain two layers of adsorbed water molecules, which are separated from the bulk liquid and are bounded to soil with distinct dielectric constant and viscosity (Figure 4b).

As pressure rises, only a monolayer of wetting liquid remains, which is adsorbed onto the soil (Philip and De Vries, 1957, reported a pressure head of -2.2×10^{-6} cm corresponding to a complete monolayer of adsorbed water). At this point, liquid water is only available in the form of discrete pockets (islands). Assuming that gradient in gravitational potential is insignificant in vapor flow, studies by Mehta et al. (1994) and Saito et al. (2006) described isothermal vapor HC (K_{vap}) as derivative of Fick's law of vapor diffusion and relative humidity,

$$K^{vap} = \frac{\rho_{sv}}{\rho_w} D \frac{Mg}{RT} H_r, \tag{20}$$

where ρ_{sv} and ρ_w are saturated vapor and water density, respectively; D is vapor diffusivity in porous media; M is molecular weight of water; g is gravitational acceleration; R is universal gas constant; T is absolute temperature; and H_r is dimensionless relative humidity. Vapor diffusivity is described as

$$D = \theta_{air} D_{air} \tau, \tag{21}$$

where θ_{air} is volumetric air content and τ is a dimensionless tortuosity factor for gas transport. Here, we use the proposed model by Moldrup et al. (1999) given as

$$\tau = \frac{\theta_{air}^{1+3/b}}{\phi^{3/b}}, \tag{22}$$

where b is Campbell (1974) pore-size distribution index obtained from soil water retention. One can replace

the parameter b with an equivalent expression of fractal dimension (Tyler & Wheatcraft, 1990); as a result, we redefine tortuosity factor as

$$\tau = \frac{\theta_{air}^{1-3(D_j-3)}}{\phi^{-3(D_j-3)}}, \tag{23}$$

where D_j is fractal dimension corresponding to the last fractal regime (j). Diffusivity of water vapor in air (D_{air}) as function of temperature is given as

$$D_{air} = 2.14\times10^{-5}\left(\frac{T}{273.15}\right)^2. \tag{24}$$

Saturated vapor density as a function of temperature is given as

$$\rho_{sv} = 10^{-3}\exp\left(31.3716-6014.79T^{-1}-7.92495\times10^{-3}T\right)T^{-1}, \tag{25}$$

and relative humidity can be determined from the Kelvin equation,

$$H_r = \exp\left(-\frac{hMg}{RT}\right). \tag{26}$$

2.5. Complete HC Model

Total HCF is described as the summation of contributions of capillary, film, and vapor flow (Lebeau & Konrad, 2010; Or & Tuller, 2000; Peters, 2013; Peters & Durner, 2008; Rudiyanto et al., 2015; Wang et al., 2016; Zheng et al., 2015),

$$K^{total} = K^{cap} + \left(1-\frac{\theta_{cap}}{\theta_s}\right)K^{ads} + K^{vap}. \tag{27}$$

The adsorptive component is multiplied by a coefficient that represents the interactions between capillary and adsorptive components. As a result, unlike the approach used by Or and Tuller (2000), this joint model eliminates additional fitting parameters used for assigning weight to each component of flow (Lebeau & Konrad, 2010). Total HC model is validated in this study using preexisting measurements obtained from the literature that extend applied pressure head to near oven dryness. Consideration of vapor diffusion has also changed classical assumptions regarding equilibrium state; thus, a larger time span is required to reach local equilibrium in laboratory and field experiments (Ouedraogo et al., 2013).

We compare the performance of our proposed model with both the unimodal capillary relative unsaturated HCF defined by Ghanbarian et al. (2016; equation 28) and the PDI model (Iden & Durner, 2014; Appandix B). The PDI water retention model includes four parameters (θ_s, θ_r, α, and n; Appendix B) to be tuned by fitting WRF to the entire range of data, and the extra empirical shape parameter m from Van Genuchten (1980) model was set to $m = 1 - 1/n$ following Iden and Durner (2014). Moreover, h_0 was set to -6.3×10^6 cm, and in cases where θ_s is known, this parameter was removed from the fitting procedure. The PDI HC model includes four parameters (K_S^{cap}, ℓ, K_S^{ads}, and a; Appendix B) that need to be tuned. Often, K_S^{cap} is measured, and ℓ takes values of 0.5, 1, and 2 representing Mualem (1976a, 1976b), Alexander and Skaggs (1986), and Burdine's (1953) models, respectively. Herein, ℓ is considered as a free parameter and is tuned according to the studied soil. The film flow conductivity equations also require estimation of h_a, K_S^{ads}, and a, where h_a (air entry value) is set as $1/\alpha$. Therefore, the PDI model requires several measurements of HC both at high (where capillary conductivity dominates flow movement) and low (where film conductivity dominates flow movement) saturation to tune these four parameters.

3. Results

3.1. Changepoint Analysis and Fitting Soil Water Retention

To detect existence of any possible changepoints within soil water retention, a scaling analysis is performed using equation (2). The bimodal and multimodal WRFs (equations (A8) and (7), respectively) and unimodal

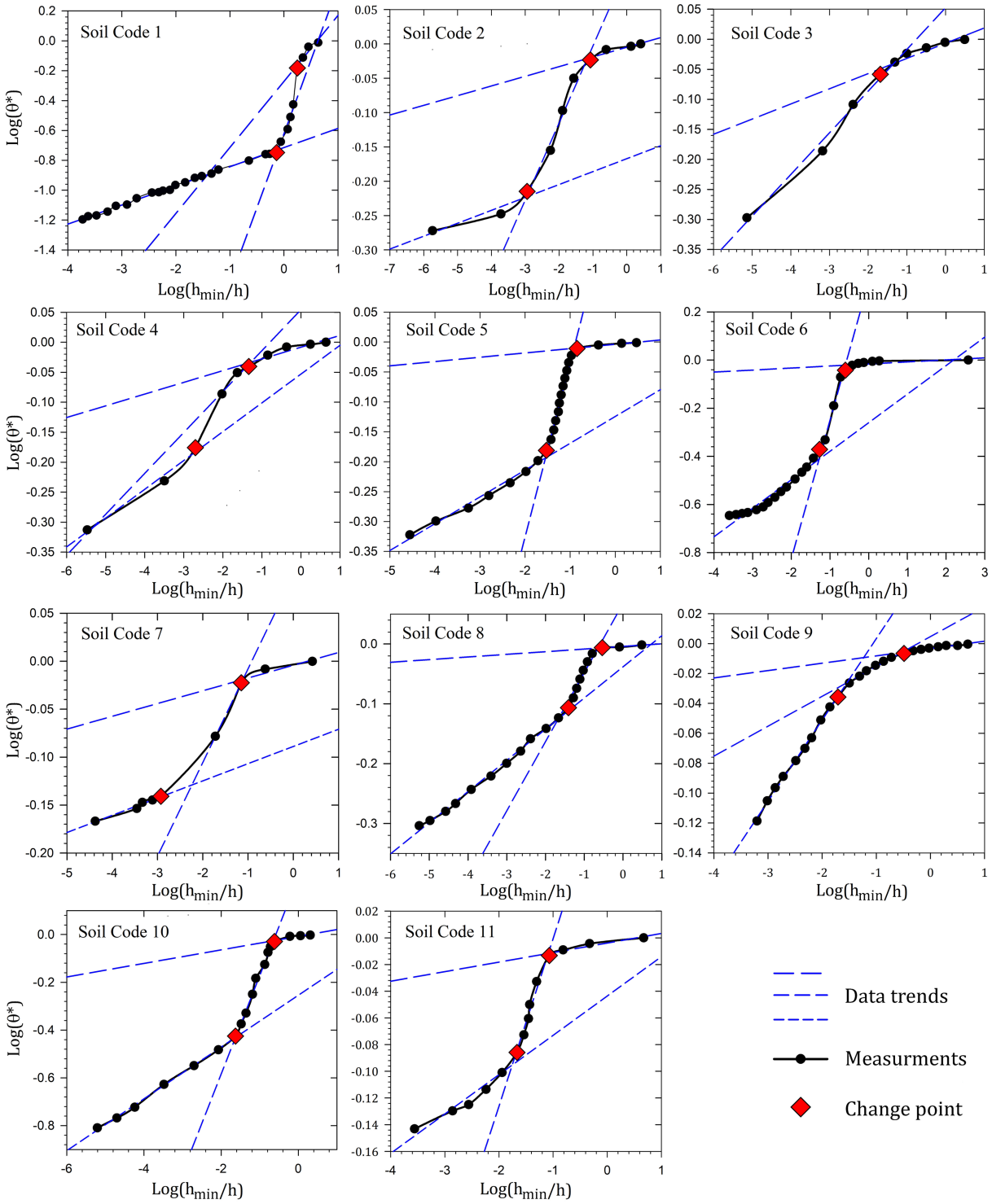

Figure 5. Log-log plots of scaled volumetric water content versus pressure head. Shifts in curve slope represents negative value of Hurst exponent or $D-3$ in terms of fractal dimension. Changes in slopes (blue dash lines) represent changes in fractal dimension of soil.

WRF equation (11) are fitted to the entire range of measured water retention data for all soil samples to evaluate the performance of the herein proposed joint HCF and the predecessor HCF (Ghanbarian et al., 2016). The obtained parameters are then used to plot log-log curves of θ^* versus (h_{min}/h). Existence of an

Table 1
Water Retention Parameters Obtained by Tuning WRF Model Against Observed Data (SI)

Soil code	Texture	Regime	Parameters				K_{sat} or $K(\theta)$ (cm/day)
			ϕ	β	$h_k\,(cm)$	D	
1	Sand	1st	0.419	0.419	11.068	2.122	673.000
		2nd	0.148	0.148	9.065	2.719	
		3rd	0.063	0.524	24.067	2.985	
2	Sandy loam	1st	0.404	0.837	2.732	2.945	9.000
		2nd	0.313	0.313	102.125	2.570	
		3rd	0.077	0.934	299.159	2.992	
3	Clay loam	1st	0.528	1.000	11.417	2.949	0.647
		2nd	0.307	1.000	299.972	2.965	
		3rd	N/A	N/A	N/A	N/A	
4	Silt loam	1st	0.530	1.000	4.660	2.948	0.278
		2nd	0.441	0.516	128.586	2.804	
		3rd	0.197	0.999	299.932	2.978	
5	Loam	1st	0.440	0.762	4.239	2.918	12.533
		2nd	0.422	0.422	28.142	2.595	
		3rd	0.180	0.182	129.564	2.804	
6	Sand	1st	0.380	0.397	6.678	2.616	108.900
		2nd	0.337	0.337	14.976	2.395	
		3rd	0.112	0.518	24.012	2.964	
7	Loamy sand	1st	0.340	0.934	4.456	2.951	55.550
		2nd	0.290	0.290	44.168	2.639	
		3rd	0.175	0.175	166.712	2.652	
8	Loam	1st	0.430	0.828	30.583	2.938	3.981
		2nd	0.418	0.447	119.592	2.797	
		3rd	0.250	0.999	299.964	2.972	
9	Clay	1st	0.555	0.999	0.005	2.992	2.754
		2nd	0.534	1.000	84.389	2.957	
		3rd	0.476	0.999	299.975	2.960	
10	Loam	1st	0.460	0.537	20.821	2.817	17.280
		2nd	0.450	0.457	51.352	2.665	
		3rd	0.125	0.958	299.745	2.985	
11	Sandy clay	1st	0.330	1.000	4.281	2.958	12.100
		2nd	0.257	0.257	68.857	2.611	
		3rd	0.151	0.403	141.289	2.931	

Note. Model parameters associated with lowest value of root mean square error among both hybrid-evolution Markov chain Monte Carlo (Sadegh et al., 2017, 2018) and local optimization approaches (Sadegh et al., 2019) are presented here.

abrupt change in the slope of the curve was used as a criterion for identifying changepoints. Using the methodology and test statistic proposed in section 2.2, and by maximizing $T(k)$, the exact location of changepoints can be determined (for a more comprehensive description, interested reader is referred to section 3.1 of ModaresiRad et al., 2019). Figure 5 illustrates the results of the proposed test statistic for all 11 soil samples used in this study. All soil samples exhibit three distinct water retention characteristics except for Soil Code 3.

3.2. Unsaturated HC

Most developed models based on fractal geometry have shown poor results when describing permeability of soils at low water contents. Hunt, Ghanbarian, et al. (2013), Hunt, Ewing, et al. (2013) discussed that HC is strongly dependent on the pore size distribution and found that their developed bimodal piecewise model was consistent with Kutílek (2004) model with an advantage of being applicable to both structural-textural and textural-textural pore combinations. Nevertheless, the adjustments they made to the capillary conductivity model based on pore size distribution cannot fully describe entire range of relation between unsaturated HC and pressure head. Processes such as film flow on surface of grains and vapor diffusivity must also be considered at low saturations. Recently, a conceptual model has been developed by Almquist et al.

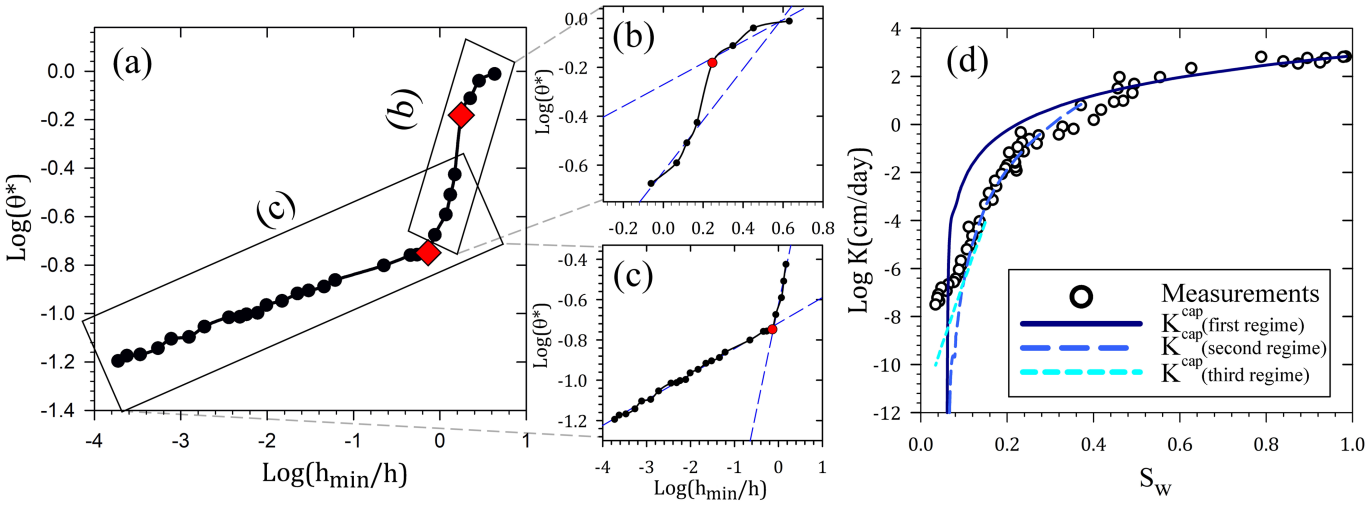

Figure 6. Multifractal analysis of HC based on changes in the slope of scaled water retention for Soil Code 1. (a) Log-log plot of the scaled water retention curve (equation (2)) with two change points (red diamonds). (b and c) Magnified sections of the curve demonstrating fractal dimension changes. (d) Modeling unsaturated HC for these three fractal regimes by deriving the required water retention parameters from equation (13) and applying them to the proposed multi fractal HCF (equation (25)).

(2018) to address the contribution of thick water films to total water retention of soil in a fractal manner; however, the model was developed and assessed on the basis of a single soil, and further research is required to assess the effectiveness of the model.

The herein proposed model requires prior and accurate knowledge about water retention and porosity, as well as a single available measurement of either saturated or near saturated HC. It is argued that having an accurate estimation of K_{sat} or $K(\theta)$ is extremely important as it works as a benchmark for prediction of other missing unsaturated hydraulic conductivities (ModaresiRad et al., 2019). Accordingly, as given in Table 1, some of the inappropriate measured values of K_{sat} from the studied soil databases were not used herein. Instead, a measurement of HC near saturation was used to fit the model (using equation (9)). The extended multimodal piecewise model of capillary flow is clearly more apt for a wider range of matric potentials and soils with multifractal properties. Log-log plot of water retention (Figure 6a) clearly describes three distinct regimes (with three different slopes, further demonstrated in Figures 6b and 6c). Accordingly, the proposed multimodal HCF was used to model HC of Soil Code 1, the results of which are presented in Figure 6d. For illustrative purposes, the range of calculated HC from each regime is extended to the highest applied pressure. Figure 6d shows that a single fractal dimension (K^{cap} from the first regime) is, in fact, incapable of describing a vast range of pressure head, whereas a multifractal approach adequately captures the complexity of the soil geometry.

On the other hand, it is evident that even though the proposed piecewise model improves fit near the dry end (Figure 6d), it still underestimates HC due to overlooking adsorptive and diffusive processes. In a study by Goss and Madliger (2007), upward diffusive vapor flux in the top layer of soil, also known as "evaporative flux into atmosphere," was calculated utilizing the Fick's law. It was found that only the top layer of soil (0–1.5 cm) contributed to upward diffusive vapor transport and that transitivity of water in lower depth of soil occurs in the form of film flow. In this study, the fractal dimension of the second regime was used to describe the tortuosity factor of gas transport for Soil Code 3 (which has two fractal regimes). For the remaining soil samples, given they have three fractal regimes, the fractal dimension of their third regime was used to describe the tortuosity factor. Figure 7 presents the outcomes of fitting the new piecewise unsaturated HC model to the studied soils, where it can be seen that in all cases, after crossing a certain pressure head, film and vapor conductivities dominate the rate of flow movement in soil. Figure 8 illustrates comparison plots of performance of models based on PDI, percolation theory (Ghanbarian et al., 2016), and the herein proposed integrated percolation theory. Comparing these three models indicates that both the proposed joint HCF and PDI models are able to describe the full range of saturation whereas the previous model proposed by

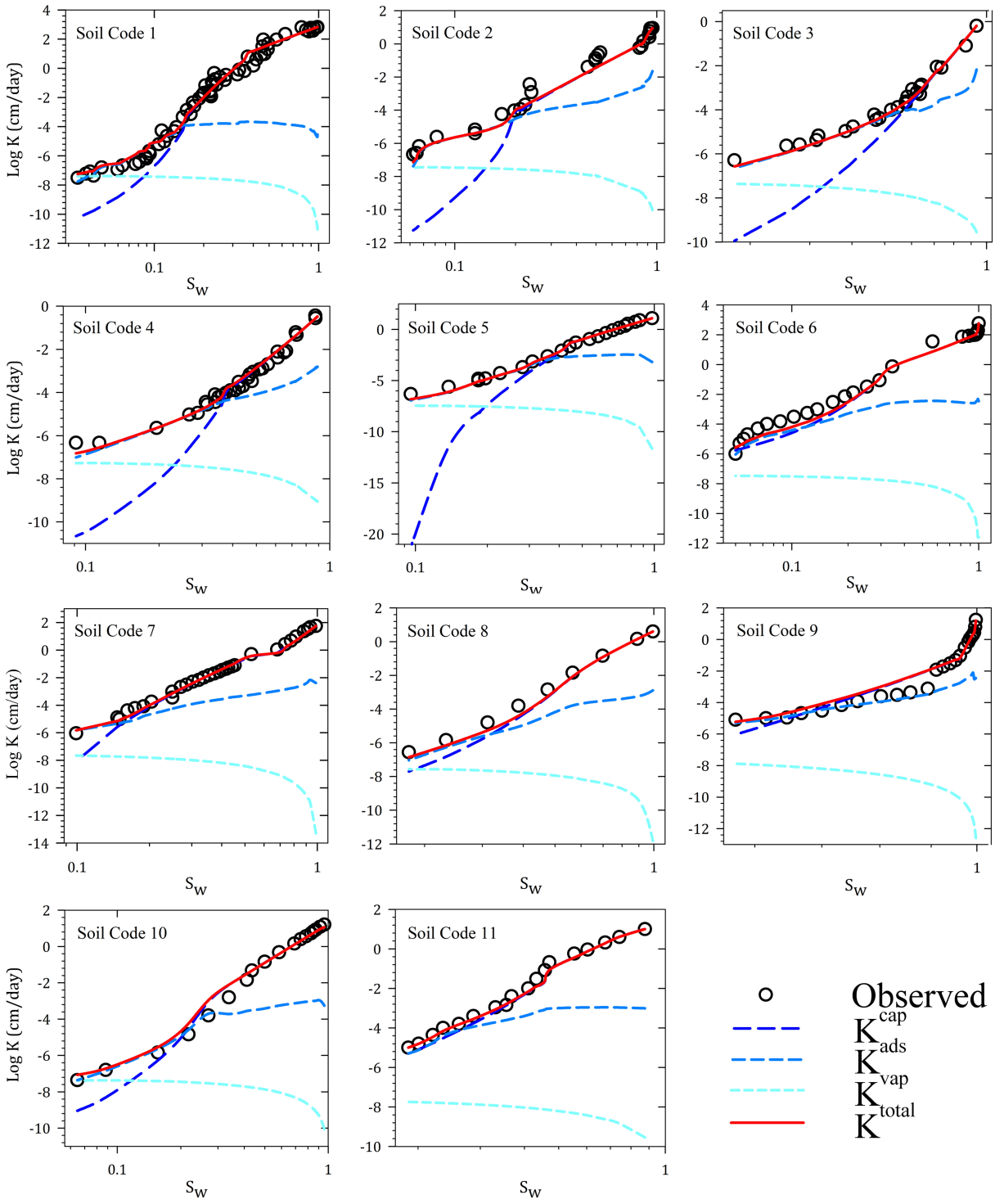

Figure 7. Hydraulic conductivity versus saturation (logarithmic scale) of observed and simulated proposed model for Soil Codes 1–11. The herein proposed joint model, K^{total} (red solid lines), is composed of a multifractal capillary flow model, K^{cap}(dark blue dashed line); film flow model, K^{ads}(light blue dashed line); and vapor flow model, K^{vap}(cyan dashed line).

Ghanbarian et al. (2016) is most reliable only around HC values of near saturation and greatly underestimates middle to dry ranges of HC. Although both PDI and the herein proposed model are accurately describing the HC curve, the PDI model uses empirical parameters that are not physically

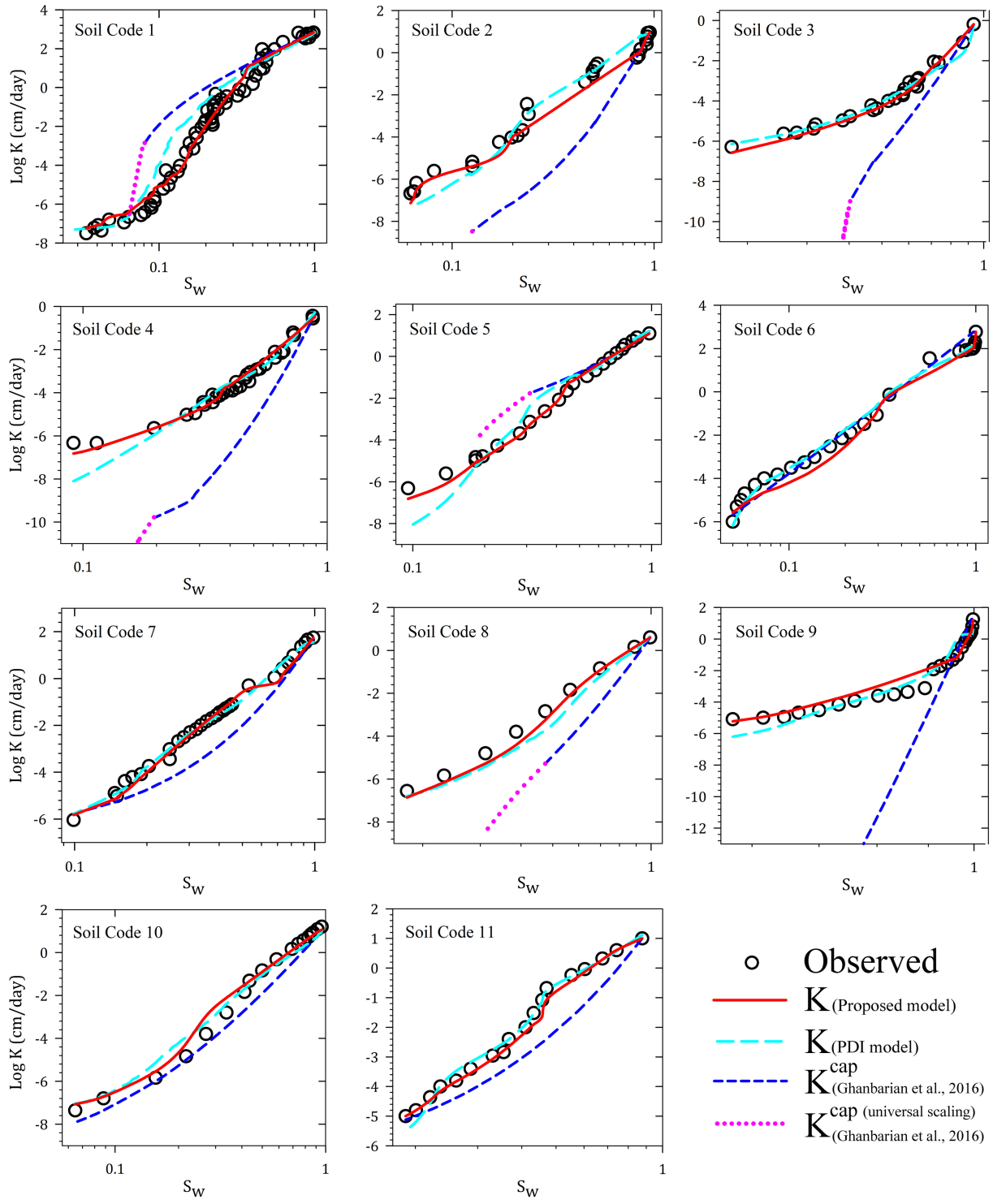

Figure 8. Observed and simulated hydraulic conductivity versus saturation (logarithmic scale) for Soil Codes 1–11. Three models of PDI (cyan dashed line), percolation theory (Ghanbarian et al., 2016; dark blue dashed line and pink dotted line), and integrated percolation theory (herein proposed model; red solid line) are drawn for each soil. Both PDI and integrated percolation theory models are comprised of capillary, film, and vapor flow components, whereas the Ghanbarian et al. (2016) model is a capillary model that utilizes universal scaling to describe conductivity below the crossover point.

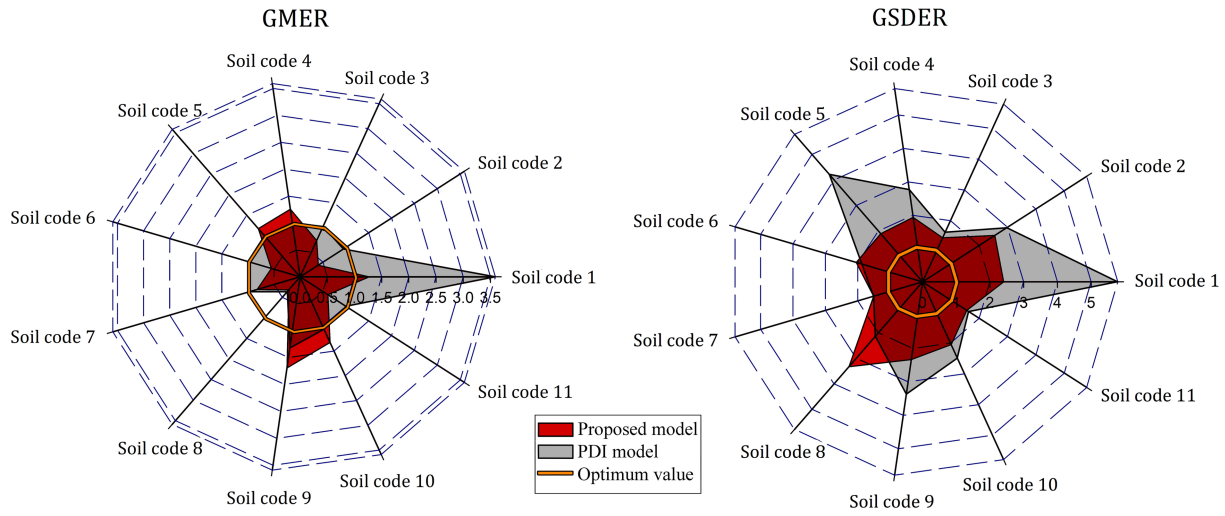

Figure 9. Goodness-of-fit criteria for the proposed integrated percolation theory model (red area) and the PDI model (gray area). The yellow decagon indicates the optimum value of each criterion. *GMER* < 1 and *GMER* > 1 indicate underestimation and overestimation of the model, and *GSDER* value of 1 denotes a perfect fit.

sound. Schaap and Leij (2000) reported negative values of the tortuosity/connectivity parameter, ℓ. Studies by Peters et al. (2011) and Peters (2014) derived lower-bound value of $\ell = -2$, indicating an increase in K_r^{cap} as S_{cap} decreases. Moreover, to determine the parameters of PDI film conductivity model (K_s^{film} and a), in addition to saturated HC measurement, a number of unsaturated HC measurements associated with dominance of film flow is required, whereas our proposed model requires only one saturated or near saturated measurement of HC.

Both bimodal and multimodal HCFs describe the measured HC well to a certain critical point, beyond which the capillary flow no longer dominates the conductivity of liquid and its value decreases sharply toward zero. As a result, the model tends to significantly underestimate HC (evident in all soil samples in Figure 7). The film conductivity model works as a complementary part of the total conductivity model and describes relatively dry regions of unsaturated HC. The contribution of the vapor conductivity model shown in Figure 7 illustrates that using the fractal dimension of the last regime to describe tortuosity factor for vapor transport through soil is clearly apt. The onset of dominance of vapor flow varies according to obtained results, and it starts to manifest itself at significantly different values of saturation depending on the soil pore space geometry. Also, we demonstrate that universal scaling (pink dotted line in Figure 8) described in numerous studies, including Ghanbarian-Alavijeh and Hunt (2012), Ghanbarian, Hunt, and Daigle (2015), Ghanbarian, Hunt, Skinner, et al. (2015), and Ghanbarian et al. (2016), in fact, is not able to describe flow processes below the crossover point (θ_x). Note that the soils without the pink dotted line did not contain measurements below 16,000 cm H_2O. The contribution of universal scaling to overall unsaturated HC was not thoroughly assessed in any of the previous studies. As discussed by Hunt, Ghanbarian, et al. (2013), Hunt, Ewing, et al. (2013), their studied experimental soils did not contain measurements sufficiently low that the universal scaling would hold and stated that typical range for universal scaling should be $0 < \theta < 0.1$, which is where the contribution of vapor diffusion is often observed. Therefore, the second term ($\theta_t < \theta < \theta_x$) of the equation (10) cannot be used to accurately describe unsaturated HC at low water contents. A more convenient approach would be to utilize the joint HCF described in this paper, which fills the gap by accounting for film and vapor flow processes.

Figure 9 illustrates goodness-of-fit results for the herein proposed HCF and the PDI model on the basis of the geometrical mean error ratio (GMER) and the geometrical standard deviation error ratio (GSDER) criteria. Predictions of the model overestimate and underestimate measured data if *GMER* > 1 and *GMER* < 1, respectively. A perfect fit is obtained once GSDER reaches its minimum value of 1. Both GMER and GSDER are superior error metrics compared to the traditionally used normalized root mean squared error and coefficient of determination (R^2) for studying HC, since they are suited for lognormally distributed data. Herein, each point is normalized by dividing prediction value by its corresponding measured value, hence

assigning a balanced impact on total error to high and low values of unsaturated HC. The GMER criterion indicates that both the proposed model and the PDI model have a low level of deviance in the prediction of unsaturated HC for all 11 studied soil samples. The GMER of the PDI model suggests existence of a balance of positive and negative errors (except for Soil Code 1 that GMER clearly shows overestimation of the PDI model) compared to the proposed joint HCF. However, GSDER values indicate that the prediction of unsaturated HC of the proposed joint HCF based on the studied soil samples (except for Soil Code 8) has a relatively lower error compared to the PDI model and is able to predict HC more accurately. Average GSDER associated with the proposed model is around 1.5, and GSDER associated with the Ghanbarian et al. (2016) model spikes to a value of 10^7 for Soil Codes 3, 4, 8, and 9 due to very low performance of the model (Figure 8), and therefore, results of error criteria of the Ghanbarian et al. (2016) model were excluded from illustration. Of all the studied data sets, Soil Codes 9 and 8 were associated with the highest bias in predictions of the joint model of unsaturated HC. These two soil samples represent the highest values of model overestimation and underestimation, respectively. Figure 7 shows that the main source of overestimation and underestimation for Soil Codes 9 and 8 is the multifractal capillary conductivity model. In both cases, it is clear that fractal properties from the second and third fractal regimes obtained from water retention data are biased, and as thoroughly discussed in ModaresiRad et al. (2019), this may stem from faulty measurements of water retention experiments.

4. Conclusions

Traditionally, unsaturated HC is modeled using the concept of bundle of tubes pore-scale models (i.e., tubes of uniform size, tubes of various sizes, intersecting tubes, and nonintersecting tubes), which only considers the capillary flow. Often, these models use empirical equations to describe the relation between HC and pressure head or volumetric water content, with parameters that generally lack physical descriptions. We propose a joint HCF that uses geometry of pore space and physics of water transport in soil to derive the mathematical relationship between HC and pressure head or volumetric water content, in which all parameters have physical description. Our proposed model extends the earlier bifractal HCFs (Hunt, Ewing, et al., 2013; Hunt, Ghanbarian, et al., 2013; ModaresiRad et al., 2019) to a multifractal HCF (three fractal regimes) that is more flexible to represent changes in soil pore size distribution. This substantially improves the flexibility of unsaturated HC curve for multifractal soils by incorporating one extra fractal regime.

The herein proposed joint HCF compensates for limitations of the capillary conductivity model from critical path analysis of percolation theory at low water contents by including contributions of film and vapor conductivity. This enhances prediction of unsaturated HC at low water contents. Performance of the proposed model was compared to its predecessor model (Ghanbarian, Hunt, & Daigle, 2015; Ghanbarian, Hunt, Skinner, et al., 2015) and the PDI model, showing that joint HCF model outperforms the other two models. Liquid transport in soil is a combination of all three types of flow (capillary, film, and vapor flow). Therefore, considering only the capillary model (Ghanbarian, Hunt, & Daigle, 2015; Ghanbarian, Hunt, Skinner, et al., 2015;Van Genuchten, 1980) can result in faulty estimations. Capillary model alone results in underestimation of unsaturated HC especially from middle to high ranges of pressure head (where film flow and vapor diffusion dominate the liquid transport rate). The two extra components of film and vapor flow significantly improve the estimation of unsaturated HC at the dry end, resulting in an accurate prediction of HC over the entire spectrum of pressure head. Moreover, our proposed joint HCF model is computationally less demanding compared to the PDI model, since our model only tunes WRF parameters, whereas the PDI model tunes both WRF and HCF parameters.

Finally, we demonstrate in this paper that the fractal dimension of the last fractal regime is an appropriate choice for modeling tortuosity of gas transport between liquid islands in vadose zone, since it captures the complexity of the pore space geometry. We further demonstrate that application of universal scaling from percolation theory (Ghanbarian-Alavijeh & Hunt, 2012; Ghanbarian et al., 2016) for prediction of HC is not recommended as moisture contents go below the crossover point (θ_x), based on a wide variety of soil textures explored. The comparison of the joint film and vapor conductivities to universal scaling from percolation theory showed the adequacy of our proposed model in predicting the dry ranges of unsaturated HC.

Acknowledgments

The authors are thankful to editor Sanchez-Villa, associate editor, and two anonymous reviewers for their thorough review of this manuscript and constructive comments. The herein used 11 data sets are collected from the published literature and are presented as supporting information.Soil Code 1 (Shonai Sand): Mehta, B. K., Shiozawa, S. H. O., & Nakano, M. (1994). Hydraulic properties of a sandy soil at low water contents. Soil Science, *157*(4), 208–214.Soil Codes 2 and 3 (Sandy Loam & Clay Loam): Tuller, M., & Or, D. (2001). Hydraulic conductivity of variably saturated porous media: Film and corner flow in angular porous media. Water Resources Research, *37*(5), 1257–1276. https://doi.org/10.1029/2000WR900328Soil Code 4 (Silt Loam): Zhang, Z. F. (2010). Soil water retention and relative permeability for full range of saturation. Pacific Northwest National Lab.(PNNL), Richland, WA (United States).Soil Codes 5, 7, 8, 9, 10, and 11 (Gilat Loam, Masa Loamy Sand, Adelanto Loam, Hollern clay 1, Pachapa Loam, & Pachapa fine Sandy Clay): Wang, Y., Ma, J., & Guan, H. (2016). A mathematically continuous model for describing the hydraulic properties of unsaturated porous media over the entire range of matric suctions. Journal of Hydrology, *541*, 873–888. https://doi.org/10.1016/j.jhydrol.2016.07.046Soil Code 6 (Plumhof I sand): Leij, F. J. (1996). *The UNSODA unsaturated soil hydraulic database: User's manual* (Vol. *96*). National Risk Management Research Laboratory, Office of Research and Development, US Environmental Protection Agency.

References

Alexander, L., & Skaggs, R. W. (1986). Predicting unsaturated hydraulic conductivity from the soil water characteristic. *Transactions of ASAE*, *29*(1), 176–184. https://doi.org/10.13031/2013.30123

Alfaro Soto, M. A., Chang, H. K., & van Genuchten, M. T. (2017). Fractal-based models for the unsaturated soil hydraulic functions. *Geoderma*, *306*(December 2016), 144–151. https://doi.org/10.1016/j.geoderma.2017.07.019

Allred, B., & Brown, G. O. (1994). Surfactant-induced reductions in soil hydraulic conductivity. *Groundwater Monitoring & Remediation*, *14*(2), 174–184. https://doi.org/10.1111/j.1745-6592.1994.tb00112.x

Almquist, V., Brueck, C., Clarke, S., Wanzek, T., & Dragila, M. I. (2018). Bioavailable water in coarse soils: A fractal approach. *Geoderma*, *323*, 146–155. https://doi.org/10.1016/j.geoderma.2018.02.036

Arya, L. M., & Paris, J. F. (1981). A physicoempirical model to predict the soil moisture characteristic from particle-size distribution and bulk density data 1. *Soil Science Society of America Journal*, *45*(6), 1023–1030. https://doi.org/10.2136/sssaj1981.03615995004500060004x

Bird, N. R. A., Perrier, E., & Rieu, M. (2000). The water retention function for a model of soil structure with pore and solid fractal distributions. *European Journal of Soil Science*, *51*(1), 55–63. https://doi.org/10.1046/j.1365-2389.2000.00278.x

Birdsell, D. T., Rajaram, H., Dempsey, D., & Viswanathan, H. S. (2015a). Hydraulic fracturing fluid migration in the subsurface: A review and expanded modeling results. *Water Resources Research*, *51*, 7159–7188. https://doi.org/10.1002/2015WR017810

Birdsell, D. T., Rajaram, H., Dempsey, D., & Viswanathan, H. S. (2015b). Numerical model of hydraulic fracturing fluid transport in the subsurface with pressure transient and density effects. In *49th US Rock Mechanics/Geomechanics Symposium*. San Francisco, California: American Rock Mechanics Association.

Birdsell, D. T., Rajaram, H., & Lackey, G. (2015). Imbibition of hydraulic fracturing fluids into partially saturated shale. *Water Resources Research*, *51*, 6787–6796. https://doi.org/10.1002/2015WR017621

Blunt, M., King, M. J., & Scher, H. (1992). Simulation and theory of two-phase flow in porous media. *Physical Review A*, *46*(12), 7680–7699. https://doi.org/10.1103/PhysRevA.46.7680

Brooks, R. H., & Corey, A. T. (1966). Properties of porous media affecting fluid flow. *Journal of the Irrigation and Drainage Division*, *92*(2), 61–90.

Buckingham, E. (1907). Studies on the movement of soil moisture. *US Dept. Agic. Bur. Soils Bull.*, *38*.

Burdine, N. (1953). Relative permeability calculations from pore size distribution data. *Journal of Petroleum Technology*, *5*(03), 71–78. https://doi.org/10.2118/225-G

Campbell, G. S. (1974). A simple method for determining unsaturated conductivity from moisture retention data. *Soil Science*, *117*(6), 311–314. https://doi.org/10.1097/00010694-197406000-00001

Campbell, G., & Shiozawa, S. (1994). Prediction of hydraulic properties of soils using particle-size distribution and bulk density data. In M. van Genuchten et al. (Eds.). *Proceedings of the International Workshop on Indirect Methods for Estimating the Hydraulic Properties of Unsaturated Soils, University of California*, *U.S. Salinity Lab., Agric. Res. Serv., U.S. Dep. of Agric., Riverside, Calif* (pp. 317–328.)

Childs, E. C., & Collis-George, N. (1950). The permeability of porous materials. *Proceedings of the Royal Society of London A*, *201*(1066), 392–405.

Derjaguin, B. V. (1987a). Some results from 50 years' research on surface forces. *Progress in Colloid and Polymer Science*, *74*(1), 17–30. https://doi.org/10.1007/BF01191008

Derjaguin, B. V. (1987b). Some results from 50 years' research on surface forces. In *Surface Forces and Surfactant Systems*, (pp. 17–30). New York: Springer.

Derjaguin, B. V. (1992). Correct form of the equation of capillary condensation in porous bodies in application to the separation of adsorption and capillary condensation in slits and porous bodies of known structure and determination of their structure by adsorption and sorption. *Progress in Surface Science*, *40*(1–4), 118–132. https://doi.org/10.1016/0079-6816(92)90038-J

Derjaguin, B. V., & Churaev, N. V. (1992). Polymolecular adsorption and capillary condensation in narrow slit pores. *Progress in Surface Science*, *40*(1–4), 173–191. https://doi.org/10.1016/0079-6816(92)90045-J

Diamantopoulos, E., & Durner, W. (2013). Physically-based model of soil hydraulic properties accounting for variable contact angle and its effect on hysteresis. *Advances in Water Resources*, *59*, 169–180. https://doi.org/10.1016/j.advwatres.2013.06.005

Durner, W. (1994). Hydraulic conductivity estimation for soils with heterogeneous pore structure. *Water Resources Research*, *30*(2), 211–223. https://doi.org/10.1029/93WR02676

Fatt, I., & Dykstra, H. (1951). Relative permeability studies. *Journal of Petroleum Technology*, *3*(09), 249–256. https://doi.org/10.2118/951249-G

Fayer, M. J., & Simmons, C. S. (1995). Earth and Environmental Sciences Center, Pacific Northwest Laboratory, Richland, Washington. *Water Resources Research*, *31*(5), 1233–1238. https://doi.org/10.1029/95WR00173

Fredlund, D. G., & Xing, A. (1994). Equations for the soil-water characteristic curve. *Canadian Geotechnical Journal*, *31*, 521–532. https://doi.org/10.1139/t94-120

Fuentes, C., Vauclin, M., Parlange, J.-Y., & Haverkamp, R. (1996). A note on the soil-water conductivity of a fractal soil. *Transport in Porous Media*, *23*(1), 31–36.

Ghanbarian, B., Hunt, A. G., & Daigle, H. (2015). Fluid flow in porous media with rough pore-solid interface. *Water Resources Research*, *52*, 2045–2058. https://doi.org/10.1002/2015WR017857

Ghanbarian, B., Hunt, A. G., Skinner, T. E., & Ewing, R. P. (2015). Saturation dependence of transport in porous media predicted by percolation and effective medium theories. *Fractals*, *23*, 1540004. https://doi.org/10.1142/S0218348X15400046

Ghanbarian-Alavijeh, B., & Hunt, A. G. (2012). Unsaturated hydraulic conductivity in porous media: Percolation theory. *Geoderma*, *187-188*, 77–84. https://doi.org/10.1016/j.geoderma.2012.04.007

Gimenez, D., Perfect, E., Rawls, W. J., & Pachepsky, Y. (1997). Fractal models for predicting soil hydraulic properties: A review. *Engineering Geology*, *48*(3–4), 161–183. https://doi.org/10.1016/S0013-7952(97)00038-0

Goss, K., & Madliger, M. (2007). Estimation of water transport based on in situ measurements of relative humidity and temperature in a dry Tanzanian soil. *Water Resources Research*, *43*, W05433. https://doi.org/10.1029/2006WR005197

Groenevelt, P. H., & Grant, C. D. (2004). A new model for the soil-water retention curve that solves the problem of residual water contents. *European Journal of Soil Science*, *55*(3), 479–485. https://doi.org/10.1111/j.1365-2389.2004.00617.x

Helba, A. A., Sahimi, M., Scriven, L. E., & Davis, H. T. (1992). Percolation theory of two-phase relative permeability. *SPE Reservoir Engineering*, *7*(01), 123–132. https://doi.org/10.2118/11015-PA

Hunt, A. G. (2001). Applications of percolation theory to porous media with distributed local conductances. *Advances in Water Resources*, *24*(3–4), 279–307. https://doi.org/10.1016/S0309-1708(00)00058-0

Hunt, A. G. (2004a). Continuum percolation theory for water retention and hydraulic conductivity of fractal soils: Estimation of the critical volume fraction for percolation. *Advances in Water Resources*, *27*(2), 175–183. https://doi.org/10.1016/j.advwatres.2003.10.004
Hunt, A. G. (2004b). Percolative transport in fractal porous media. *Chaos, Solitons and Fractals*, *19*(2), 309–325. https://doi.org/10.1016/S0960-0779(03)00044-4
Hunt, A. G., Ewing, R. P., & Horton, R. (2013). What's wrong with soil physics? *Soil Science Society of America Journal*, *77*(6), 1877–1887. https://doi.org/10.2136/sssaj2013.01.0020
Hunt, A. G., & Gee, G. W. (2002a). Application of critical path analysis to fractal porous media: Comparison with examples from the Hanford site. *Advances in Water Resources*, *25*(2), 129–146. https://doi.org/10.1016/S0309-1708(01)00057-4
Hunt, A. G., & Gee, G. W. (2002b). Water-retention of fractal soil models using continuum percolation theory. *Vadose Zone Journal*, *1*(2), 252–260. https://doi.org/10.2136/vzj2002.2520
Hunt, A. G., Ghanbarian, B., & Saville, K. C. (2013). Unsaturated hydraulic conductivity modeling for porous media with two fractal regimes. *Geoderma*, *207-208*(1), 268–278. https://doi.org/10.1016/j.geoderma.2013.05.023
Hunt, A. G., & Skinner, T. E. (2005). Hydraulic conductivity limited equilibration: Effect on water retention characteristics. *Vadose Zone Journal*, *4*(1), 145–150. https://doi.org/10.2113/4.1.145
Iden, S. C., & Durner, W. (2014). Comment on "simple consistent models for water retention and hydraulic conductivity in the complete moisture range" by A. Peters. *Water Resources Research*, *50*, 7530–7534. https://doi.org/10.1002/2014WR015937
Ippisch, O., Vogel, H. J., & Bastian, P. (2006). Validity limits for the van Genuchten-Mualem model and implications for parameter estimation and numerical simulation. *Advances in Water Resources*, *29*(12), 1780–1789. https://doi.org/10.1016/j.advwatres.2005.12.011
Israelachvili, J. N. (2011). *Intermolecular and surface forces*. Burlington, MA: Academic press.
Iwamatsu, M., & Horii, K. (1996). Capillary condensation and adhesion of two wetter surfaces. *Journal of Colloid and Interface Science*, *182*(2), 400–406. https://doi.org/10.1006/jcis.1996.0480
Jacquin, C. G., & Adler, P. M. (1985). The fractal dimension of a gas-liquid interface in a porous medium. *Journal of Colloid and Interface Science*, *107*(2), 405–417. https://doi.org/10.1016/0021-9797(85)90193-6
Jansik, D. P., Wildenschild, D., & Rosenberg, N. D. (2011). Flow processes in the dry regime: The effect on capillary barrier performance. *Vadose Zone Journal*, *10*(4), 1173–1184. https://doi.org/10.2136/vzj2010.0128
Kebre, M. B., Cherblanc, F., Ouedraogo, F., Jamin, F., Naon, B., Zougmore, F., & Benet, J. C. (2017). Water flow in soil at small water contents: A simple approach to estimate the relative hydraulic conductivity in sandy soil. *European Journal of Soil Science*, *68*(2), 167–176. https://doi.org/10.1111/ejss.12408
Kelleners, T. J., Koonce, J., Shillito, R., Dijkema, J., Berli, M., Young, M. H., et al. (2016). Numerical modeling of coupled water flow and heat transport in soil and snow. *Soil Science Society of America Journal*, *80*(2), 247–263. https://doi.org/10.2136/sssaj2015.07.0279
Khlosi, M., Cornelis, W. M., Douaik, A., van Genuchten, M. T., & Gabriels, D. (2008). Performance evaluation of models that describe the soil water retention curve between saturation and oven dryness. *Vadose Zone Journal*, *7*(1), 87–96. https://doi.org/10.2136/vzj2007.0099
Kosugi, K. (1996). Lognormal distribution model for unsaturated soil hydraulic properties. *Water Resources Research*, *32*(9), 2697–2703. https://doi.org/10.1029/96WR01776
Kutílek, M. (2004). Soil hydraulic properties as related to soil structure. *Soil and Tillage Research*, *79*(2 SPEC.ISS), 175–184. https://doi.org/10.1016/j.still.2004.07.006
Langmuir, I. (1938). Repulsive forces between charged surfaces in water, and the cause of the Jones-Ray effect. *Science*, *88*(2288), 430–432. https://doi.org/10.1126/science.88.2288.430
Larson, R. G., Scriven, L. E., & Davis, H. T. (1981). Percolation theory of two phase flow in porous media. *Chemical Engineering Science*, *36*(1), 57–73. https://doi.org/10.1016/0009-2509(81)80048-6
Lebeau, M., & Konrad, J.-M. (2010). A new capillary and thin film flow model for predicting the hydraulic conductivity of unsaturated porous media. *Water Resources Research*, *46*, W12554. https://doi.org/10.1029/2010WR009092
Lehmann, P., Assouline, S., & Or, D. (2008). Characteristic lengths affecting evaporative drying of porous media. *Physical Review E*, *77*, 056309. https://doi.org/10.1103/PhysRevE.77.056309
Leij, F. J. (1996). *The UNSODA unsaturated soil hydraulic database: user's manual* (Vol. 96). Ada, Oklahoma, United States: National Risk Management Research Laboratory, Office of Research and Development, US Environmental Protection Agency.
Li, K. (2010). More general capillary pressure and relative permeability models from fractal geometry. *Journal of Contaminant Hydrology*, *111*(1–4), 13–24. https://doi.org/10.1016/j.jconhyd.2009.10.005
Li, K., & Horne, R. N. (2005). An analytical model for production decline-curve analysis in naturally fractured reservoirs. *SPE Reservoir Evaluation and Engineering*, *8*(03), 197–204. https://doi.org/10.2118/83470-PA
Mason, G., & Morrow, N. (1986). Meniscus displacement curvatures of a perfectly wetting liquid in capillary pore throats formed by spheres. *Journal of Colloid and Interface Science*, *109*(1), 46–56. https://doi.org/10.1016/0021-9797(86)90280-8
Mehta, B. K., Shiozawa, S. H. O., & Nakano, M. (1994). Hydraulic properties of a sandy soil at low water contents. *Soil Science*, *157*(4), 208–214. https://doi.org/10.1097/00010694-199404000-00002
Millington, R. J., & Quirk, J. P. (1961).Permeability of porous solids, *Transactions of the Faraday Society*. *57*: 1200-1207.
ModaresiRad, A., Ghahraman, B., & Sadegh, M. (2019). Revising tortuosity and multi-fractal assumptions of unsaturated hydraulic conductivity from critical path analysis of percolation theory. *Geoderma*, *352*, 213–227. https://doi.org/10.1016/j.geoderma.2019.06.002
Moldrup, P., Olesen, T., Yamaguchi, T., Schjønning, P., & Rolston, D. E. (1999). Modeling diffusion and reaction in soils: IX. The Buckingham-Burdine-Campbell equation for gas diffusivity in undisturbed soil. *Soil Science*, *164*(8), 542–551. https://doi.org/10.1097/00010694-199908000-00002
Mualem, Y. (1976a). A new model for predicting the hydraulic conductivity of unsaturated porous media. *Water Resources Research*, *12*(3), 513–522. https://doi.org/10.1029/WR012i003p00513
Mualem, Y. (1976b). catalogue of the hydraulic properties of unsaturated soils.
Or, D., & Assouline, S. (2013). The foam drainage equation for unsaturated flow in porous media. *Water Resources Research*, *49*, 6258–6265. https://doi.org/10.1002/wrcr.20525
Or, D., & Tuller, M. (1999). Liquid retention and interfacial area in variably saturated porous media: Upscaling from single-pore to sample-scale model. *Water Resources Research*, *35*, 3591–3605. https://doi.org/10.1029/1999WR900262
Or, D., & Tuller, M. (2000). Flow in unsaturated fractured porous media: Hydraulic conductivity of rough surfaces. *Water Resources Research*, *36*(5), 1165–1177. https://doi.org/10.1029/2000WR900020
Ouedraogo, F., Cherblanc, F., Naon, B., & Bénet, J.-C. (2013). Water transfer in soil at low water content. Is the local equilibrium assumption still appropriate? *Journal of Hydrology*, *492*, 117–127. https://doi.org/10.1016/j.jhydrol.2013.04.004

Penman, H. L. (1940). Gas and vapour movements in the soil: I. The diffusion of vapours through porous solids. *The Journal of Agricultural Science*, *30*(3), 437–462. https://doi.org/10.1017/S0021859600048164

Perrier, E., Bird, N., & Rieu, M. (1999). Generalizing the fractal model of soil structure: The pore–solid fractal approach. *Geoderma*, *88*(3–4), 137–164. https://doi.org/10.1016/S0016-7061(98)00102-5

Peters, A. (2013). Simple consistent models for water retention and hydraulic conductivity in the complete moisture range. *Water Resources Research*, *49*, 6765–6780. https://doi.org/10.1002/wrcr.20548

Peters, A. (2014). Reply to comment by Iden, D. and Durner, W. on 'Simple consistent models for water retention and hydraulic conductivity in the complete moisture range'. *Water Resources Research*, *50*, 7535–7539. https://doi.org/10.1002/2014WR016107

Peters, A., & Durner, W. (2008). A simple model for describing hydraulic conductivity in unsaturated porous media accounting for film and capillary flow. *Water Resources Research*, *44*, W11417. https://doi.org/10.1029/2008WR007136

Peters, A., Durner, W., & Wessolek, G. (2011). Consistent parameter constraints for soil hydraulic functions. *Advances in Water Resources*, *34*(10), 1352–1365. https://doi.org/10.1016/j.advwatres.2011.07.006

Philip, J. R. (1977). Unitary approach to capillary condensation and adsorption. *The Journal of Chemical Physics*, *66*(11), 5069–5075. https://doi.org/10.1063/1.433814

Philip, J. R., & De Vries, D. A. (1957). Moisture movement in porous materials under temperature gradients. *Eos, Transactions American Geophysical Union*, *38*(2), 222–232. https://doi.org/10.1029/TR038i002p00222

Purcell, W. R. (1949). Capillary pressures-their measurement using mercury and the calculation of permeability therefrom. *Journal of Petroleum Technology*, *1*(02), 39–48. https://doi.org/10.2118/949039-G

Resurreccion, A. C., Moldrup, P., Tuller, M., Ferré, T. P. A., Kawamoto, K., Komatsu, T., & De Jonge, L. W. (2011). Relationship between specific surface area and the dry end of the water retention curve for soils with varying clay and organic carbon contents. *Water Resources Research*, *47*, W06522. https://doi.org/10.1029/2010WR010229

Rieu, M., & Sposito, G. (1991). Fractal fragmentation, soil porosity, and soil water properties: I. Theory. *Soil Science Society of America Journal*, *55*(5), 1231–1238. https://doi.org/10.2136/sssaj1991.03615995005500050006x

Ross, B. (1986). Dispersion in fractal fracture networks. *Water Resources Research*, *22*(5), 823–827. https://doi.org/10.1029/WR022i005p00823

Rossi, C., & Nimmo, J. R. (1994). Modeling of soil water retention from saturation to oven dryness. *Water Resources*, *30*(3), 701–708. https://doi.org/10.1029/93WR03238

Rudiyanto, Sakai, M., Van Genuchten, M. T., Alazba, A. A., Setiawan, B. I., & Minasny, B. (2015). A complete soil hydraulic model accounting for capillary and adsorptive water retention, capillary and film conductivity, and hysteresis. *Water Resources Research*, *51*, 8757–8772. https://doi.org/10.1002/2015WR017703

Sadegh, M., AghaKouchak, A., Flores, A., Mallakpour, I., & Nikoo, M. R. (2019). A multi-model nonstationary rainfall-runoff modeling framework: Analysis and toolbox. *Water Resources Management*, *33*(9), 3011–3024. https://doi.org/10.1007/s11269-019-02283-y

Sadegh, M., Majd, M. S., Hernandez, J., & Haghighi, A. T. (2018). The quest for hydrological signatures: Effects of data transformation on Bayesian inference of watershed models. *Water Resources Management*, *32*(5), 1867–1881. https://doi.org/10.1007/s11269-018-1908-6

Sadegh, M., Ragno, E., & AghaKouchak, A. (2017). Multivariate Copula Analysis Toolbox (MvCAT): Describing dependence and underlying uncertainty using a Bayesian framework. *Water Resources Research*, *53*, 5166–5183. https://doi.org/10.1002/2016WR020242

Sadeghi, M., Ghahraman, B., Ziaei, A. N., Davary, K., & Reichardt, K. (2012). Invariant solutions of Richards' equation for water movement in dissimilar soils. *Soil Science Society of America Journal*, *76*, 30799. https://doi.org/10.2136/sssaj2011.0275

Saito, H., Šimůnek, J., & Mohanty, B. P. (2006). Numerical analysis of coupled water, vapor, and heat transport in the vadose zone. *Vadose Zone Journal*, *5*(2), 784–800. https://doi.org/10.2136/vzj2006.0007

Sakai, M., Toride, N., & Šimůnek, J. (2009). Water and vapor movement with condensation and evaporation in a sandy column. *Soil Science Society of America Journal*, *73*(3), 707–717. https://doi.org/10.2136/sssaj2008.0094

Schaap, M. G., & Leij, F. J. (2000). Improved prediction of unsaturated hydraulic conductivity with the Mualem-van Genuchten model. *Soil Science Society of America Journal*, *64*(3), 843–851. https://doi.org/10.2136/sssaj2000.643843x

Schneider, M., & Goss, K. U. (2012). Prediction of water retention curves for dry soils from an established pedotransfer function: Evaluation of the Webb model. *Water Resources Research*, *48*, W06603. https://doi.org/10.1029/2011WR011049

Shepard, J. S. (1993). Using a fractal model to compute the hydraulic conductivity function. *Soil Science Society of America Journal*, *57*(2), 300–306. https://doi.org/10.2136/sssaj1993.03615995005700020002x

Shokri, N., & Or, D. (2010). Comment on "A simple model for describing hydraulic conductivity in unsaturated porous media accounting for film and capillary flow" by A. Peters and W. Durner. *Water Resources Research*, *46*, W06801. https://doi.org/10.1029/2009WR008917

Soto, M. A., & Vilar, O. M. (2006). Evaluation of a pore fractal model for the prediction of soil water retention curve. In *Unsaturated Soils 2006* (pp. 2441–2452), Reston, Virginia: American Society of Civil Engineers.

Tiktak, A., Hendriks, R. F. A., Boesten, J., & Van der Linden, A. M. A. (2012). A spatially distributed model of pesticide movement in Dutch macroporous soils. *Journal of Hydrology*, *470-471*, 316–327. https://doi.org/10.1016/j.jhydrol.2012.09.025

Tokunaga, T. K. (2009). Hydraulic properties of adsorbed water films in unsaturated porous media. *Water Resources Research*, *45*, W06415. https://doi.org/10.1029/2009WR007734

Tuller, M., & Or, D. (2001). Hydraulic conductivity of variably saturated porous media: Film and corner flow in angular porous media. *Water Resources Research*, *37*(5), 1257–1276. https://doi.org/10.1029/2000WR900328

Tuller, M., & Or, D. (2005). Water films and scaling of soil characteristic curves at low water contents. *Water Resources Research*, *41*, 09403. https://doi.org/10.1029/2005WR004142

Tuller, M., Or, D., & Dudley, L. M. (1999). Adsorption and capillary condensation in porous media: Liquid retention and interfacial configurations in angular pores. *Water Resources Research*, *35*(7), 1949–1964. https://doi.org/10.1029/1999WR900098

Tyler, S. W., & Wheatcraft, S. W. (1990). Fractal processes in soil water retention. *Water Resources Research*, *26*(5), 1047–1054. https://doi.org/10.1029/WR026i005p01047

Van Genuchten, M. T. (1980). A closed-form equation for predicting the hydraulic conductivity of unsaturated soils 1. *Soil Science Society of America Journal*, *44*(5), 892–898. https://doi.org/10.2136/sssaj1980.03615995004400050002x

Vink, J. P. M., Gottesbüren, B., Diekkrüger, B., & van der Zee, S. E. (1997). Simulation and model comparison of unsaturated movement of pesticides from a large clay lysimeter. *Ecological Modelling*, *105*(1), 113–127. https://doi.org/10.1016/S0304-3800(97)00147-6

Wang, Y., Ma, J., & Guan, H. (2016). A mathematically continuous model for describing the hydraulic properties of unsaturated porous media over the entire range of matric suctions. *Journal of Hydrology*, *541*, 873–888. https://doi.org/10.1016/j.jhydrol.2016.07.046

Wang, Y., Ma, J., Guan, H., & Zhu, G. (2017). Determination of the saturated film conductivity to improve the EMFX model in describing the soil hydraulic properties over the entire moisture range. *Journal of Hydrology*, *549*, 38–49. https://doi.org/10.1016/j.jhydrol.2017.03.063

Wang, Y., Ma, J., Zhang, Y., Zhao, M., & Edmunds, W. M. (2013). A new theoretical model accounting for film flow in unsaturated porous media. *Water Resources Research*, *49*, 5021–5028. https://doi.org/10.1002/wrcr.20390

Weber, T. K. D., Iden, S. C., & Durner, W. (2017). Unsaturated hydraulic properties of Sphagnum moss and peat reveal trimodal pore-size distributions. *Water Resources Research*, *53*, 415–434. https://doi.org/10.1002/2016WR019707

Wyllie, M. R. J., & Gardner, G. H. F. (1958). The generalized Kozeny-Carman equation. *World Oil*, *146*(4), 121–128.

Zand-Parsa, S. (2006). Improved soil hydraulic conductivity function based on specific liquid-vapour interfacial area around the soil particles. *Geoderma*, *132*(1–2), 20–30. https://doi.org/10.1016/j.geoderma.2005.04.020

Zand-Parsa, S., & Sepaskhah, A. R. (2004). Soil hydraulic conductivity function based on specific liquid-vapor interfacial area around the soil particles. *Geoderma*, *119*(1–2), 143–157. https://doi.org/10.1016/S0016-7061(03)00258-1

Zhang, Z. F. (2010). Soil water retention and relative permeability for full range of saturation. Pacific Northwest National Lab.(PNNL), Richland, WA (United States).

Zhang, Z. F. (2011). Soil water retention and relative permeability for conditions from oven-dry to full saturation. *Vadose Zone Journal*, *10*(4), 1299–1308. https://doi.org/10.2136/vzj2011.0019

Zheng, W., Yu, X., & Jin, Y. (2015). Considering surface roughness effects in a triangular pore space model for unsaturated hydraulic conductivity. *Vadose Zone Journal*, *14*, 1539–1663. https://doi.org/10.2136/vzj2014.09.0121

Appendix A: Derivation of The Multifractal Water Retention And HC

For applied pressure head (h), $h_{k2} < h < h_{max}$ (third regime) expressions for WRF is defined as

$$\theta = \beta_3 \frac{3-D_3}{r_{k2}^{3-D_3}} \int_{r_{min}}^{r} r^3 r^{-1-D_3} dr = \beta_3 \left[\left(\frac{r}{r_{k2}} \right)^{3-D_3} - \left(\frac{r_{min}}{r_{k2}} \right)^{3-D_3} \right], \tag{A1}$$

where θ is volumetric water content and D_3 and β_3 are fractal dimension and PSF water retention parameter of the third regime, respectively. Since PSF model is an iterative process of partitioning a bounded region in a Euclidian space, the fractal volume is divided into three portions of p for pore, s for solid, and f for fractal at each iteration. Therefore, the total volume of the bounded region is the summation of pores, solids, and fractals, and the proportions of these three add up to one ($p+s+f = 1$). Given the definition of PSF model, the parameter β can be described as $\beta = p/(p+s)$. Similarly, for the second regime ($h_{k1} < h < h_{k2}$), θ would be

$$\begin{aligned} \theta &= \beta_2 \frac{3-D_2}{r_{k1}^{3-D_2}} \int_{r_{k2}}^{r} r^3 r^{-1-D_2} dr + \beta_3 \frac{3-D_3}{r_{k2}^{3-D_3}} \int_{r_{min}}^{r_{k2}} r^3 r^{-1-D_3} dr \\ &= \beta_2 \left[\left(\frac{r}{r_{k1}} \right)^{3-D_2} - \left(\frac{r_{k2}}{r_{k1}} \right)^{3-D_2} \right] + \beta_3 \left[\left(\frac{r_{k2}}{r_{k2}} \right)^{3-D_3} - \left(\frac{r_{min}}{r_{k2}} \right)^{3-D_3} \right] = \beta_2 \left[\left(\frac{r}{r_{k1}} \right)^{3-D_2} - \left(\frac{r_{k2}}{r_{k1}} \right)^{3-D_2} \right] + \phi_3, \end{aligned} \tag{A2}$$

where D_2 and β_2 are fractal dimension and PSF water retention parameter of the second regime, respectively, and ϕ_3 is porosity of the third regime ($h_{min} < h < h_{k1}$). For the first regime, we have

$$\begin{aligned} \theta &= \beta_1 \frac{3-D_1}{r_{max}^{3-D_1}} \int_{r_{k1}}^{r} r^3 r^{-1-D_1} dr + \beta_2 \frac{3-D_2}{r_{k1}^{3-D_2}} \int_{r_{k2}}^{r_{k1}} r^3 r^{-1-D_2} dr + \beta_3 \frac{3-D_3}{r_{k2}^{3-D_3}} \int_{r_{min}}^{r_{k2}} r^3 r^{-1-D_3} dr \\ &= \beta_1 \left[\left(\frac{r}{r_{max}} \right)^{3-D_1} - \left(\frac{r_{k1}}{r_{max}} \right)^{3-D_1} \right] + \beta_2 \left[\left(\frac{r_{k1}}{r_{k1}} \right)^{3-D_2} - \left(\frac{r_{k2}}{r_{k1}} \right)^{3-D_2} \right] + \beta_3 \left[\left(\frac{r_{k2}}{r_{k2}} \right)^{3-D_3} - \left(\frac{r_{min}}{r_{k2}} \right)^{3-D_3} \right] \\ &= \beta_1 \left[\left(\frac{r}{r_{max}} \right)^{3-D_1} - \left(\frac{r_{k1}}{r_{max}} \right)^{3-D_1} \right] + \phi_2 + \phi_3, \end{aligned} \tag{A3}$$

where D_1 and β_1 are fractal dimension and PSF water retention parameter of the first regime and ϕ_2 is the porosity of the second regime. Now, considering that the porosities of the first, second, and third regions are defined as

$$\phi_1 = \beta_1\left[1-\left(\frac{r_{k1}}{r_{max}}\right)^{3-D_1}\right], \tag{A4}$$

$$\phi_2 = \beta_2\left[1-\left(\frac{r_{k2}}{r_{k1}}\right)^{3-D_2}\right], \text{and} \tag{A5}$$

$$\phi_3 = \beta_3\left[1-\left(\frac{r_{min}}{r_{k2}}\right)^{3-D_3}\right], \tag{A6}$$

respectively, and utilizing Young-Laplace equation the piecewise multifractal soil WRF is derived as

$$\theta = \begin{cases} \phi, & h<h_{min} \\ \phi-\beta_1\left[1-\left[\frac{h}{h_{min}}\right]^{D_1-3}\right], & h_{min}<h<h_{k1} \\ \phi_2+\phi_3-\beta_2\left[1-\left[\frac{h}{h_{k1}}\right]^{D_2-3}\right], & h_{k1}<h<h_{k2} \\ \phi_3-\beta_3\left[1-\left[\frac{h}{h_{k2}}\right]^{D_3-3}\right], & h_{k2}<h<h_{max} \end{cases} \tag{A7}$$

and according to Hunt, Ghanbarian, et al. (2013), Hunt, Ewing, et al. (2013), the piecewise soil water retention model for two fractal regimes is given as

$$\theta = \begin{cases} \phi, & h<h_{min} \\ \phi-\beta_1\left[1-\left[\frac{h}{h_{min}}\right]^{D_1-3}\right], & h_{min}<h<h_k \\ \phi_2+\beta_2\left[1-\left[\frac{h}{h_k}\right]^{D_2-3}\right]. & h_k<h<h_{max} \end{cases} \tag{A8}$$

The critical volume content of percolation θ_t from critical path analysis in fully saturated case can be written as (Hunt, Ewing, et al., 2013; Hunt, Ghanbarian, et al., 2013)

$$\theta_t = \beta_1\frac{3-D_1}{r_{max}^{3-D_1}}\int_{r_{c(\theta=\phi)}}^{r_{max}} r^3 r^{-1-D_1}dr = \beta_1\left[1-\left(\frac{r_{c(\theta=\phi)}}{r_{max}}\right)^{3-D_1}\right]. \tag{A9}$$

Combining equations (A7) and (A9) for a condition that $\theta_t < \phi_1+\phi_2$ yields the critical pore radius r_c given $\theta = \phi$,

$$r_{c(\theta=\phi)} = r_{max}\left[\frac{\beta_1-\theta_t}{\beta_1}\right]^{\frac{1}{3-D_1}}. \tag{A10}$$

In an unsaturated condition and a case where $\theta - \theta_t > \phi_2$, according to Hunt, Ghanbarian, et al. (2013), Hunt, Ewing, et al. (2013),

$$r_{c(\theta)} = r_{max}\left[\frac{\beta_1-\phi+\theta-\theta_t}{\beta_1}\right]^{\frac{1}{3-D_1}}, \tag{A11}$$

and for a case in which $\phi_2 > \theta - \theta_t > \phi_3$,

$$r_{c(\theta)} = r_{k1}\left[\frac{\beta_2-\phi_2+\theta-\theta_t}{\beta_2}\right]^{\frac{1}{3-D_2}}. \tag{A12}$$

Also for a case of $\theta - \theta_t < \phi_3$ we define θ_t as

$$\theta_t = \beta_3 \frac{3-D_3}{r_{k2}^{3-D_3}} \int_{r_c(\theta)}^{r} r^3 r^{-1-D_3} dr = \beta_3 \left[\left(\frac{r}{r_{k2}} \right)^{3-D_3} - \left(\frac{r_c(\theta)}{r_{k2}} \right)^{3-D_3} \right], \tag{A13}$$

and

$$r_{c(\theta)} = r_{k2} \left[\frac{\beta_3 - \phi_3 + \theta - \theta_t}{\beta_3} \right]^{\frac{1}{3-D_3}}. \tag{A14}$$

Furthermore, the ratio of radii corresponding to the second and first changepoints can be defined by setting equation (A3) equal to equation (A7) for $h_{min} < h < h_{k1}$, which results in

$$\frac{r_{k1}}{r_{max}} = \left[\frac{\beta_1 - \phi_1}{\beta_1} \right]^{\frac{1}{3-D_1}}, \tag{A15}$$

and by setting equation (A2) equal to equation (A7) for $h_{k1} < h < h_{k2}$, which results in

$$\frac{r_{k2}}{r_{k1}} = \left[\frac{\beta_2 - \phi_2}{\beta_2} \right]^{\frac{1}{3-D_2}}. \tag{A16}$$

Multiplying ratios in equations (A15) and (A16) determines

$$\frac{r_{k2}}{r_{max}} = \left[\frac{\beta_1 - \phi_1}{\beta_1} \right]^{\frac{1}{3-D_1}} \times \left[\frac{\beta_2 - \phi_2}{\beta_2} \right]^{\frac{1}{3-D_2}}. \tag{A17}$$

Relative unsaturated HC normalized by saturated HC is described by Hunt, Ghanbarian, et al. (2013), Hunt, Ewing, et al. (2013) and modified in ModaresiRad et al. (2019) as

$$\frac{K(\theta)}{K_s} = \frac{g_c(\theta)}{g_c(\theta = \phi)} = \frac{r_c^{\lambda}(\theta)}{r_c^{\lambda}(\theta = \phi)}. \tag{A18}$$

where $\lambda = 2(4 - D_s) - ((3 - D_s/2D_s - 2) + ((1/\Omega) \times (2D_s - 4/D_s - 1)))$ and $\Omega = \ln(0.15/h)/\ln(0.15/h_{min})$. Utilizing equations (A11), (A12), (A14), and (A18) combined with the expression of ratios in equations (A15), (A16), and (A17), the piecewise multifractal relative unsaturated HCF is described as

$$K_r^{cap} = \frac{K\theta}{K_s\theta} = \begin{cases} \left[\dfrac{\beta_1 - \phi + \theta - \theta_t}{\beta_1 - \theta_t} \right]^{\frac{\lambda_1}{3-D_1}}, & \theta - \theta_t > \phi_2 + \phi_3 \\ \dfrac{\beta_1^{\frac{\lambda_1}{3-D_1}}}{\beta_2^{\frac{\lambda_2}{3-D_2}}} \left\{ \dfrac{\beta_1 - \phi_1}{\beta_1} \right\}^{\frac{\lambda_1}{3-D_1}} \dfrac{[\beta_2 - \phi_2 + \theta - \theta_t]^{\frac{\lambda_2}{3-D_2}}}{[\beta_1 - \theta_t]^{\frac{\lambda_1}{3-D_1}}}, & \phi_3 < \theta - \theta_t < \phi_2 + \phi_3 \\ \dfrac{\beta_1^{\frac{\lambda_1}{3-D_1}}}{\beta_3^{\frac{\lambda_3}{3-D_3}}} \left\{ \dfrac{\beta_1 - \phi_1}{\beta_1} \right\}^{\frac{\lambda_1}{3-D_1}} \left\{ \dfrac{\beta_2 - \phi_2}{\beta_2} \right\}^{\frac{\lambda_2}{3-D_2}} \dfrac{[\beta_3 - \phi_3 + \theta - \theta_t]^{\frac{\lambda_3}{3-D_3}}}{[\beta_1 - \theta_t]^{\frac{\lambda_1}{3-D_1}}}. & \theta - \theta_t < \phi_3 \end{cases} \tag{A19}$$

Similarly, for cases that measurement of saturated HC is not available, we have

$$K_r^{cap}=\frac{K\theta}{K\theta'}=\begin{cases}\left[\dfrac{\beta_1-\phi+\theta-\theta_t}{\beta_1-\phi+\theta'-\theta_t}\right]^{\frac{\lambda_1}{3-D_1}}, & \theta-\theta_t>\phi_2+\phi_3\\ \dfrac{\beta_1^{\frac{\lambda_1}{3-D_1}}}{\beta_2^{\frac{\lambda_2}{3-D_2}}}\left\{\dfrac{\beta_1-\phi_1}{\beta_1}^{\frac{\lambda_1}{3-D_1}}\dfrac{[\beta_2-\phi_2+\theta-\theta_t]^{\frac{\lambda_2}{3-D_2}}}{[\beta_1-\phi+\theta'-\theta_t]^{\frac{\lambda_1}{3-D_1}}}\right., & \phi_3<\theta-\theta_t<\phi_2+\phi_3\\ \dfrac{\beta_1^{\frac{\lambda_1}{3-D_1}}}{\beta_3^{\frac{\lambda_3}{3-D_3}}}\left\{\dfrac{\beta_1-\phi_1}{\beta_1}^{\frac{\lambda_1}{3-D_1}}\left\{\dfrac{\beta_2-\phi_2}{\beta_2}^{\frac{\lambda_2}{3-D_2}}\dfrac{[\beta_3-\phi_3+\theta-\theta_t]^{\frac{\lambda_3}{3-D_3}}}{[\beta_1-\phi+\theta'-\theta_t]^{\frac{\lambda_1}{3-D_1}}}\right.\right., & \theta-\theta_t<\phi_3\end{cases} \tag{A20}$$

The bimodal piecewise relative unsaturated HC model according to Hunt, Ghanbarian, et al. (2013), Hunt, Ewing, et al. (2013) is written as follows:

$$K_r=\frac{K\theta}{K_s\theta}=\begin{cases}\left[\dfrac{\beta_1-\phi+\theta-\theta_t}{\beta_1-\theta_t}\right]^{\frac{\lambda_1}{3-D_1}}, & \theta-\theta_t>\phi_2\\ \dfrac{\beta_1^{\frac{\lambda_1}{3-D_1}}}{\beta_2^{\frac{\lambda_2}{3-D_2}}}\left\{\dfrac{\beta_1-\phi_1}{\beta_1}^{\frac{\lambda_1}{3-D_1}}\dfrac{[\beta_2-\phi_2+\theta-\theta_t]^{\frac{\lambda_2}{3-D_2}}}{[\beta_1-\theta_t]^{\frac{\lambda_1}{3-D_1}}}\right., & \theta-\theta_t<\phi_2\end{cases} \tag{A21}$$

Appendix B: Water Retention and HC Model of PDI

According to Iden and Durner (2014), the water retention model of all pressure heads can be written as the summation of capillary and adsorptive water contents.

$$\theta(h)=\theta_{cap}(h)+\theta_{ads}(h)=(\theta_s-\theta_r)S_{cap}(h)+\theta_r S_{ads}(h), \tag{B1}$$

where θ_{cap} is the volumetric water contents of capillary water with saturation defined as S_{cap} and θ_{ads} is the volumetric water contents of adsorptive water with saturation defined as S_{ads}. The saturated capillary component was defined by rescaling any of the standard capillary functions, such that for Van Genuchten (1980) model S_{cap} was written as

$$S_{cap}(h)=\frac{\Gamma(h)-\Gamma(h_0)}{1-\Gamma(h_0)}, \tag{B2}$$

where h_0 is the largest value of the applied pressure head that is often assumed to be -10^7cm and $\Gamma(h)$ is the Van Genuchten (1980) WRF described as

$$\Gamma(h)=\left[\frac{1}{1+(\alpha|h|)^n}\right]^m. \tag{B3}$$

Here α,n, and m are the empirical shape parameters. The adorative saturation was proposed as a smooth piecewise linear function.

$$S_{ads}(h) = 1 + \frac{1}{x_a - x_0}\left\{x - x_a + b.\ln\left[1 + \exp\left(\frac{x_a - x}{b}\right)\right]\right\}, \tag{B4}$$

$$x = \log_{10}(|h|), \tag{B5}$$

$$x_0 = \log_{10}(|h_0|), \tag{B6}$$

$$x_a = \log_{10}(|h_a|), \tag{B7}$$

$$b = 0.1 + \frac{0.2}{n^2}\left\{1 - \exp\left[-\left(\frac{\theta_r}{\theta_s - \theta_r}\right)^2\right]\right\}. \tag{B8}$$

According to Peters (2014), the scaled relative HC function using Van Genuchten (1980) model can be written as

$$K_r^{cap} = (S^{cap})^{\ell}\left(1 - \left(\frac{1 - \Gamma(h)^{\frac{1}{m}}}{1 - \Gamma(h_0)^{\frac{1}{m}}}\right)^m\right)^2, \tag{B9}$$

in which ℓ is a dimensionless shape parameter that is associated with tortuosity of water movement path (Mualem, 1976a). Peters (2013) proposed the relative film HC as

$$K_r^{film} = \left(\frac{h_0}{h_a}\right)^{a(1 - S_{ads})}, \tag{B10}$$

where a is an empirical parameter. The isothermal vapor HC model used in PDI model is described in equations (20)–(26) except that the authors used Millington and Quirk (1961) description of tortuosity factor in the gaseous phase

$$\tau = \frac{\theta_{air}^{7/3}}{\phi^2}. \tag{B11}$$

Considering the reflected contributions of capillary, adsorptive, and vapor conductivity (equations (B9), (B10), and (20)), the total HC was described as

$$K_{total} = K_S^{cap} \times K_r^{cap} + K_S^{ads} \times K_r^{ads} + K^{vap}. \tag{B12}$$